

# Evaluation of the METRIC and TSEB remote sensing evapotranspiration models in the floodplain area of the Thaya and Morava Rivers

Authors: T. Ghisi <sup>a, b, \*</sup>, M. Fischer <sup>a, b</sup>, H. Nieto <sup>c</sup>, N. Kowalska <sup>a</sup>, G. Jocher <sup>a</sup>, L. Homolová <sup>a</sup>, V. Burchard <sup>c</sup>, Z. Žalud <sup>a, b</sup>, M. Trnka <sup>a, b</sup>

<sup>a</sup> *Global Change Research Institute of the Czech Academy of Sciences, Belidla 986/4b, 603 00 Brno, Czech Republic*

<sup>b</sup> *Mendel University in Brno, Institute of Agrosystems and Bioclimatology, Zemědělská 1, 613 00 Brno, Czech Republic*

<sup>c</sup> *Institute of Agricultural Sciences-CSIC, Serrano 115 b, 28006 Madrid, Spain*

\*Corresponding author: E-mail address: ghisi.t@czechglobe.cz (T. Ghisi).

*„As the funder requires the full Open Access to the research results of our team, we would like to apply the CC-BY-SA licence and the full Open Access option.”*

## Preprint statement

This version of the manuscript was submitted on **January 27, 2024, to the Journal of Hydrology: Regional Studies** and returned with a major revision statement. A subsequent improved version has been accepted for publication (now in proofreading as of April 24, 2024) and should be published with the DOI number: <https://doi.org/10.1016/j.ejrh.2024.101785> in the coming weeks.

## **Abstract**

**Study region:** Floodplain ecosystem region at the confluence of the Morava and Thaya Rivers, Czech Republic.

**Study focus:** Accurate determination of actual evapotranspiration ( $ET_a$ ) is essential for understanding surface hydrological conditions. The aim of this study was to evaluate two remote sensing models, METRIC and TSEB, for estimating  $ET_a$  and energy fluxes in two ecosystems using the eddy covariance (EC) as a reference.

**New hydrological insights for the region:** Both models demonstrate the ability to quantify  $ET_a$  across the region. Compared with the METRIC, which had a mean bias error (MBE) = 0.12 mm/day, the TSEB better detected  $ET_a$  in the forest test site ( $MBE_{TSEB} = -0.03$  mm/day). In contrast, the METRIC improved detection of  $ET_a$  ( $MBE_{METRIC} = -0.03$  mm/day) in grassland test site, where the TSEB overestimate daily  $ET_a$  ( $MBE_{TSEB} = 0.52$  mm/day). The models and EC indicate similar seasonal dynamics of the evaporative fraction and Bowen ratio throughout the growing season. Despite the overall agreement between the models and EC, the selected spatial outputs indicate some disagreement among them in terms of the spatial patterns of  $ET_a$ . This disagreement is related to the sensitivity of TSEB to canopy height/roughness, as well as the a priori Priestley-Taylor coefficient in forests. Despite these shortcomings, this study highlights the applicability of remote sensing energy balance-based diagnostic models for studying hydrological processes in a spatially distributed manner.

**Key words:** Eddy covariance, Evapotranspiration, Floodplain ecosystem, Remote sensing models, Water balance

# 1 Introduction

Climate projections estimate an increasing probability of extreme meteorological and climatic event occurrences, including droughts and floods, in Central Europe (Možný et al., 2020). In light of climate change, water availability is critical for maintaining agronomic production in the lowlands of Central Europe (Trnka et al., 2022a). Currently, a broad range of adaptations are being planned to mitigate the negative impacts of climate change in the area (Hlásny et al., 2014; Komissarov and Klik 2020). Considering the negative climatic water balance in the lowlands (Duethmann and Blöschl; 2018; Trnka et al., 2022b; Fischer et al., 2023), there is a need for an appropriate tool to spatially detect  $ET_a$  at the landscape level. This approach is vital for enhancing the refinement of key strategic measures aimed at managing the water balance at different spatial scales.

Remote sensing (RS) appears to be a suitable tool for assessing landscape water balance because satellite sensors can easily identify relevant land surface state variables and properties needed to model water and energy fluxes (Anderson et al., 2012), and archives can be used to perform time series analyses. While direct *in situ* evapotranspiration measurements of  $ET_a$ , such as the EC method, are focused on the individual ecosystem scale, remote sensing models allow local mapping of  $ET_a$  to the global landscape as a whole while maintaining the possibility of analyzing individual ecosystems and their role in catchment hydrology (Allen et al., 2007a; Guzinski et al., 2020).

Physically based remote sensing models based on surface energy balance principle have been widely used for the spatial estimation of  $ET_a$  (Norman et al., 1995; Anderson et al., 1997; Bastiaanssen et al., 1998; Allen et al., 2007a; Senay et al., 2007). Prominent energy balance models include one-source energy balance models such as the SEBAL (surface energy balance algorithm for land) (Bastiaanssen et al., 1998; Bastiaanssen et al., 2005) or METRIC (mapping evapotranspiration at high resolution with internalized calibration) (Allen et al., 2007a); two-source energy balance (TSEB) models (Norman et al., 1995); and three-source energy balance models (Burchard-Levine et al., 2022).

The METRIC model (Allen et al., 2007a) is based on the pioneering foundation of the SEBAL model, which uses two anchor pixels (“dry and wet pixels”) to determine the aerodynamic resistance and near-surface vertical air temperature gradient between these two extreme endmembers. The main advantage of the METRIC model is its self-calibration across the studied domain, which simplifies some physical processes, prevents difficult-to-solve errors and is less sensitive to uncertainties in land surface temperature retrievals (French, Hunsaker and Thorp, 2015). This approach makes it a suitable tool for the robustness and estimation of  $ET_a$  in areas with less known surface conditions (Chirouze et al., 2014). Compared to the METRIC model, the TSEB model uses a more detailed parameterization of the energy fluxes between the plant canopy and the soil surface. As such, the model is able to estimate transpiration from vegetation cover and evaporation from the soil surface, which can be useful within an agronomic sector where irrigation strategies strive to reduce water losses from evaporation more than from transpiration (Burchard-Levine et al., 2022). The TSEB requires a more detailed characterization of surface biophysical conditions and is more sensitive to possible errors in land surface temperature estimation (French, Hunsaker and Thorp, 2015).

Both models have demonstrated the ability to accurately detect  $ET_a$  within various ecosystems and under various environmental conditions (Allen et al., 2007b; Hankerson et al., 2012; Mkhwanazi and Chávez, 2012; Carrasco-Benavides et al., 2014; Zhang et al., 2015; Liebert et al., 2016; Nieto et al., 2019a, b; Guzinski and Nieto, 2019; Guzinski et al., 2023). However, in Central Europe, the application of the METRIC and TSEB models has been limited to only a handful of proof-of-concept studies (Fischer et al., 2023; Ghisi et al., 2023). Furthermore, although remote sensing models are generally often evaluated against the eddy covariance (EC) method, these comparisons sporadically use multiple vegetation covers for evaluation within the area of interest. This study aimed to evaluate the METRIC and TSEB models at two test sites representing different ecosystems of the southern Moravia floodplain area in the Czech Republic. Both of the selected models determine  $ET_a$  through surface energy balance yet by adopting different sets of assumptions and different levels of complexity. The selected test sites equipped with EC systems represent structurally and aerodynamically contrasting land covers—grassland and forest—ensuring a robust experimental design to evaluate remote sensing methods and their potential for hydrological studies in regions where  $ET_a$  represents the dominant water balance component.

## 2 Methods

### 2.1 Study area

The area of interest is located in the largest floodplain forest complex in the southernmost part of the South Moravia region, in the Czech Republic, near the confluence of the Thaya and Morava Rivers (Fig. 1). The elevation of the area varies between 150 and 160 m. Fluvial soils are the dominant soil type in the area. The area includes two EC stations monitoring two structurally contrasting ecosystems—forest and grassland. The 130-km<sup>2</sup> region, nicknamed the “Moravian Amazon”, represents the wedge of floodplain forest in the confluence area and is considered to become the 27<sup>th</sup> Protected Landscape Area in the Czech Republic. The forest test site (Forest) is located in a mature floodplain forest of English oak (*Quercus robur* L.), European ash (*Fraxinus angustifolia* L.) and Hornbeam (*Carpinus betulus* L.). The site is equipped with a flux tower with meteorological sensors at different heights (Kowalska et al., 2020), including an EC system (Tab 1). The Forest site contributes to the ICOS (Integrated Carbon Observation System) network. The grassland test site (Grassland) is located in the floodplain meadow approximately 850 m from the Thaya River and approximately 3 km northward from the Forest. A similar EC system is installed at a height of 2 m above the ground (Tab. 1). Although a significant part of the floodplain forest is inundated regularly during flood events or during the artificial release of flow waves from the Nové Mlýny reservoir, both test sites typically remain a few meters above the flood line.

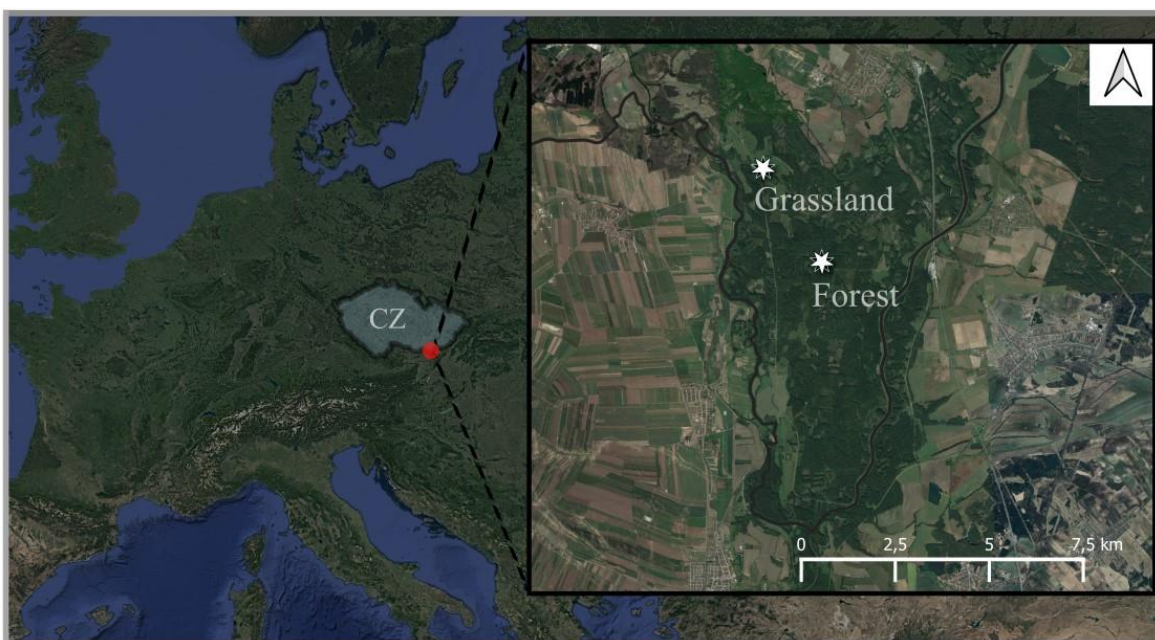


Fig. 1 Location of the floodplain area with Grassland and Forest test sites.

## 2.2 Meteorological and eddy covariance data

The METRIC and TSEB models require instantaneous meteorological data at the satellite overpass time. The meteorological station data from the Forest (36 m height) in the period 2015–2021 were used for both models at half-hourly steps. While EC data were measured at a height of 44 m, meteorological data from a height of 36 m were used as inputs to models because these data provide a continuous time series of meteorological data compared to those measured at 44 m, where meteorological data missed during some parts of the monitored period. Both the METRIC and TSEB models used the same meteorological data as the inputs except a precipitation which were required only by the METRIC model to simulate soil moisture in the hot pixel where we assumed non-zero values of  $ET_a$ . (Tab. 1).

While the data from the Forest site were available since 2015, the measurements from the Grassland began in June 2019; thus, the data were available since that period. The two EC systems used in the study were equipped with various ancillary instruments (Tab. 1).

The instrumentation used in the study fulfilled the standards of the ICOS, which provides high-quality long-term observations of greenhouse gases and greenhouse gas exchange (<https://www.icos-cp.eu/>).

Tab. 1 Instruments for measuring meteorological and EC parameters and their application during the monitored period in the Forest and Grassland.

Site	Measured parameter	Instrument	Height/Depth (m)	Monitored period
Meteorological data (Forest)	Radiation balance ( $W/m^2$ )	CNR4 Net Radiometer, Kipp&Zonen, NE	44	2015–2021
	Air temperature ( $^{\circ}C$ )	EMS33, CZ [1], HMP155, Vaisala, FI [2]	36	2015–June 2019 [1] June 2019–2021 [2]
	Wind speed (m/s)	Wind Sonic 2D, Gill Instruments, UK	36	2015–2021
	Relative humidity (%)	EMS33, CZ [1], HMP155, Vaisala, FI [2]	36	2015–June 2019 [1] June 2019–2021 [2]
	Precipitation (mm)	Thies Laser Precipitation Monitor, DE [1]	44	July 2016–2021 [1]
Rain Gauge		44	2015–July 2016	
Forest [1]; Grassland [2]	Soil heat flux ( $W/m^2$ )	HFP01SC-05, Hukseflux, NE	0.05	2015–2021 [1] June 2019–2021 [2]
Eddy covariance Forest [1] [2]; Grassland [3]	Sensible heat flux ( $W/m^2$ ) Latent heat flux ( $W/m^2$ )	Gas analyzer Li-7200 (LI-COR Environmental, Lincoln, NE); 3D sonic anemometer Gill HS-50 (Gill Instruments, Hampshire, UK)	44 [1] 48 [2] 2 [3]	2015–December 2018 [1] 2018 December–October 2021 [2] 2021 October–December 2021 [1] June 2019–2021 [3]

### Turbulent energy flux calculation and postprocessing

Turbulent energy fluxes determined by the EC method were calculated with the software EddyPro® (version 6.2.0; LI-COR Biosciences, Lincoln, NE, USA). All required corrections of the calculated covariances between the vertical wind component  $w$  and the quantity of interest, i.e.,  $H_2O$  concentrations and sonic temperature, were applied to derive the final 30-minute averaged latent (LE) and sensible heat (H) turbulent energy fluxes. The data were processed according to standard FLUXNET processing methods (Pastorello et al., 2014). This includes, for example, filtering via a friction velocity threshold (Papale et al., 2006) to ensure sufficient turbulent mixing and filtering via quality flags (Foken et al., 2004) that test the data for stationarity and turbulence development, two of the main preconditions of the EC method. This procedure ensures the highest possible quality of the used EC data. The uncertainty range of EC data of highest quality is 10–20% (Foken, 2008). Flux data gap filling was performed using the R package REddyProc (Wutzler et al., 2018), applying marginal distribution sampling (Reichstein et al., 2005). In this study, the average daily footprints of EC for both test sites in the period between 2015 and 2021 (Fig. 2) were utilized for the calculation of EC and model outputs. The footprint size for the Forest was 0.690 km<sup>2</sup>, and for the Grassland, it was 0.020 km<sup>2</sup> (Fig. 2).



Fig. 2 The average daily footprint of all available EC data of the Forest site (left) and Grassland site (right). The black lines represent cumulative contribution to measured  $ET_a$  starting from 10% around the tower (dark red color), through 30%, 50%, 70%, up to a 90% polygon (light blue color).

These EC data supplemented by soil heat flux ( $G$ ) and net radiation ( $R_n$ ) were used for the evaluation of both the METRIC and TSEB models. At both test sites,  $G$  was measured at a depth of 0.05 m, and no

measurements of soil heat storage above the heat flux plate were conducted. The EC energy fluxes of LE and H are not corrected for energy balance closure (EBC), and the residual energy was significant in some cases. The average residual energy was 38% in the Forest and 30% in the Grassland during the days from 2015 to 2021 with available satellite images. For this reason, the comparison of model-projected fluxes with EC measurements was conducted both without EBC and with EBC adjustment. The EBC adjustment was calculated according to the Bowen ratio adjustment (Twine et al., 2000; Foken 2008; Fischer et al., 2018). This method fully closes the energy balance by distributing the residual available energy to H and LE while preserving their ratio, i.e., the Bowen ratio  $H/LE$ .

### **2.3 Evapotranspiration models**

The METRIC model (Allen et al., 2007a), available at <https://github.com/midread/water>, and TSEB model (Norman et al., 1995), with code available at <https://github.com/hectornieto/pyTSEB> (<https://doi.org/10.5281/zenodo.594732>), are diagnostic remote sensing models that estimate spatial  $ET_a$  based on surface energy balance calculations using satellite land surface temperature (LST) retrieval. Although both models are based on the calculation of the surface energy balance, their approaches differ. The METRIC model is a one-source model that utilizes so-called cold and hot pixels for internal calibration to evaluate the surface temperature gradient between the land surface and air. The cold pixel characterizes moister conditions, where the surface temperature is minimal and the LAI is maximal; hence, the instantaneous LE should be the highest within the analyzed domain. Conversely, hot pixels characterize dry conditions, where the surface temperature is maximal, the LAI is minimal, and the LE should be the lowest (Allen et al., 2007a). In this study, automatic selection of hot and cold pixels (Olmedo et al., 2016) was performed.

The TSEB model is a two-source model with an emphasis on partitioning fluxes into canopy and soil categories; thus, more detailed characteristics of the canopy, such as green and total LAI, effective leaf size, and soil and leaf spectra, are needed. The TSEB physically relates the radiometric temperature acquired with thermal infrared satellite sensors to the aerodynamic temperature (defined as the extrapolation of air temperature profile down to an effective height within the canopy at which the vegetation components of sensible and latent heat flux arise (Kalma and Jupp, 1990)) required to

accurately derive H without the need for using an excess resistance formulation typical for one-source models (Kustas et al., 2016). The TSEB model uses an a priori guess of the Priestley-Taylor coefficient ( $\alpha$ ), which is iteratively reduced within the model under stressed conditions until realistic canopy and soil energy fluxes are achieved (i.e., fluxes  $\geq 0$ ), yielding the determination of the energy flux partitioning at the end of the iteration. The value of the  $\alpha$  coefficient is set to 1.26 for lower vegetation (grasslands, crops). In the forested areas,  $\alpha$  coefficient is scaled according to the study of Guzinski et al. (2013) after the work of Komatsu (2005), who focused on categorizing the  $\alpha$  coefficient in forested areas according to canopy height.

Both models calculate daily  $ET_a$  values from instantaneous values at the time of satellite overpass, but both utilize a different approach in this study. The concept behind the METRIC model assumes that the ratio between the instantaneous  $ET_a$  and the instantaneous reference evapotranspiration ( $ET_o$ ) remains constant throughout the day. Therefore, the METRIC model calculates the daily  $ET_a$  by using the reference fraction ( $ET_a / ET_o$ ) determined at the satellite overpass time. This fraction is then multiplied by the daily  $ET_o$  value (Allen et al., 2007a).

On the other hand, in the TSEB model, the total amount of latent energy (LE) is assumed to be directly proportional to the amount of incoming solar radiation. Therefore, this scaling concept initially calculates the daily LE value by computing the ratio between LE and shortwave solar incoming radiation, which is subsequently multiplied by the daily incoming solar radiation. The daily LE, expressed in energy units, is subsequently converted to  $ET_a$ , expressed in terms of mm/day.

## **2.4 Satellite data preprocessing**

In this study, Landsat 8 data were used to estimate  $ET_a$  and energy fluxes at a 30-m resolution during the period between 2015–2021. Landsat imagery was downloaded from the United States Geological Survey (USGS) Earth Explorer website (<https://earthexplorer.usgs.gov/>). The surface reflectance and surface temperature datasets from OLI+ and TIRS retrieved from Landsat Collection 2 Level 2 Science products were selected according to the occurrence of cloud cover over the area of interest. If clouds were present only partly, the cloudy pixels were filtered, and only cloud-free pixels were subsequently used. In total, 117 clear-sky images were available for the area of interest between 2015–2021.

## **2.5 Determining the momentum roughness and canopy height in the models**

Both models require the determination of a momentum roughness length ( $z_{0m}$ ) for accurate calculation of H. A concept for determining the momentum roughness differs for forested (forests) and grassed (grasslands, crops) areas. The Corine Land Cover 2018 (ESA. CORINE Land Cover 2018) dataset was used to distinguish different land cover types.

The momentum roughness calculated in both the TSEB and METRIC models for forests, as described by Raupach et al. (1994), is based on canopy height and LAI. In this study, canopy height was estimated using the Global Forest Canopy Height data (Potapov et al., 2021), which was derived from Global Ecosystem Dynamics Investigation Ecosystem (GEDI) Level 3 data (Dubayah et al., 2021) and has been operational aboard the International Space Station.

In the case of herbaceous cover (grasslands, crops),  $z_{0m}$  was scaled without determining canopy height in either model. It was assumed that the crop height varies with the LAI and that  $z_{0m}$  was directly defined according to Tasumi (2003), where  $z_{0m}$  was expressed as the LAI multiplied by 0.018.

## **2.6 Estimation of albedo, LAI and delta temperature**

The albedo is quantified as the proportion of incident shortwave radiation reflected back into the atmosphere, calculated as the ratio of reflected to incoming solar radiation. This albedo estimation was conducted using satellite bands spanning from 2015 to 2021 at both sites. The LAI, as a critical biophysical characteristic of the surface, was spatially determined utilizing data from the Landsat 8 satellite. The methodology for LAI derivation aligns with procedures established for Sentinel satellite data, employing canopy radiative transfer models as outlined in Weiss et al. (2000). This LAI estimate was further integrated into the METRIC and TSEB models, enhancing the detection and analysis of vegetation parameters. Furthermore, the concept of the delta temperature ( $\Delta T$ ) was introduced, representing the difference between the surface temperature and air temperature (recorded at 36 m above ground) over the period from 2015 to 2021.

### **3.6 Gap-filling of daily $ET_a$ using clear-sky images**

In this study, the daily  $ET_a$  outputs of both model outputs were interpolated and approximated to annual values. The available  $ET_a$  data of models were interpolated using the  $ET_a/ET_o$  ratio. The calculated  $ET_a/ET_o$  ratios were used for linear interpolation for dates between available model outputs. Then, the interpolated daily  $ET_a/ET_o$  ratios were multiplied by  $ET_o$  values to derive the gap-filled  $ET_a$ .

### 3 Results

#### 3.1 Surface conditions

The variation in albedo (Fig. 3 a) was related to seasonal variability during the year and corresponded well to the variation in the LAI in the Forest (Fig. 1 b). A greater albedo was detected in the Grassland with a maximum (0.19) in June 2017. The monthly LAI values ranged between 0.5 in the dormant season and nearly 8 during the growing season in the Forest. Lower LAI values were detected at the Grassland station, where average monthly values mostly range between 0.5 and 4. The lower LAI values were influenced by regular site management in the Grassland, which involves a regular reduction in grass cutting, consequently leading to a reduction in vegetation at the site during the year.  $\Delta T$  (Fig. 1 c) exhibited relatively low variation ranging between  $-5$  and  $5^{\circ}\text{C}$  in the Forest; however, more pronounced seasonal variability was observed in the Grassland, where  $\Delta T$  ranged from  $-1$  to  $15^{\circ}\text{C}$ . The higher values of  $\Delta T$  in the Grassland indicate a relatively high surface heating during summer periods. Also, the high  $\Delta T$  in the Grassland could be related to differences in microclimatic conditions between surfaces where air temperature was measured above forest cover and surface temperature measured at grassland. These variables represent a wide range of surface conditions at the two different EC sites, in which the TSEB and METRIC models were evaluated during the period 2015–2021.

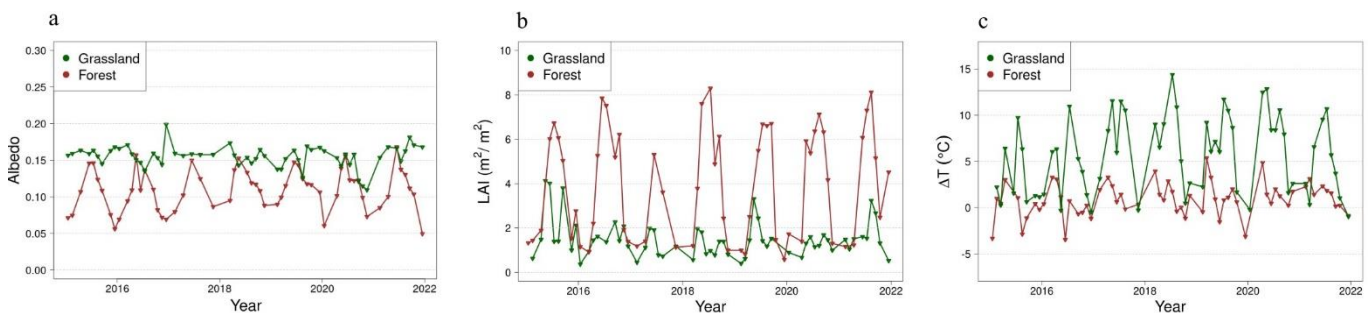


Fig. 3 Temporal variation of albedo (a), LAI (b) and  $\Delta T$  (c) at the Forest (brown lines) and Grassland (green lines).  $\Delta T$  shown a difference between surface temperature and air temperature.

#### 4.2 Evaluation of TSEB and METRIC to EC measurement

Instantaneous energy flux values obtained through the two models were compared with those obtained through the EC method without EBC adjustment. These comparisons were made between the TSEB model and EC (Fig. 4 a, c) and between the METRIC model and EC (Fig. 4 b, d) at satellite overpass

times for the Forest and Grassland. Overall, good agreement was observed between the TSEB model and EC method for H ( $MBE_{TSEB} = 26.77 \text{ W/m}^2$ ,  $R^2_{TSEB} = 0.37$ ) and for LE ( $MBE_{TSEB} = 38.4 \text{ W/m}^2$ ,  $R^2_{TSEB} = 0.60$ ) in the Forest (Fig. 4 a). Similarly, compared with the EC method, the METRIC model (Fig. 4 b) tended to overestimate H ( $MBE_{METRIC} = 64.2 \text{ W/m}^2$ ,  $R^2_{METRIC} = 0.19$ ), LE ( $MBE_{METRIC} = 76.04 \text{ W/m}^2$ ,  $R^2_{METRIC} = 0.54$ ), and  $R_n$  ( $MBE_{METRIC} = 77.62 \text{ W/m}^2$ ,  $R^2_{METRIC} = 0.85$ ). The METRIC model also estimated a few negative LE values, indicating a condensation process on the surface. These values corresponded to the winter months.

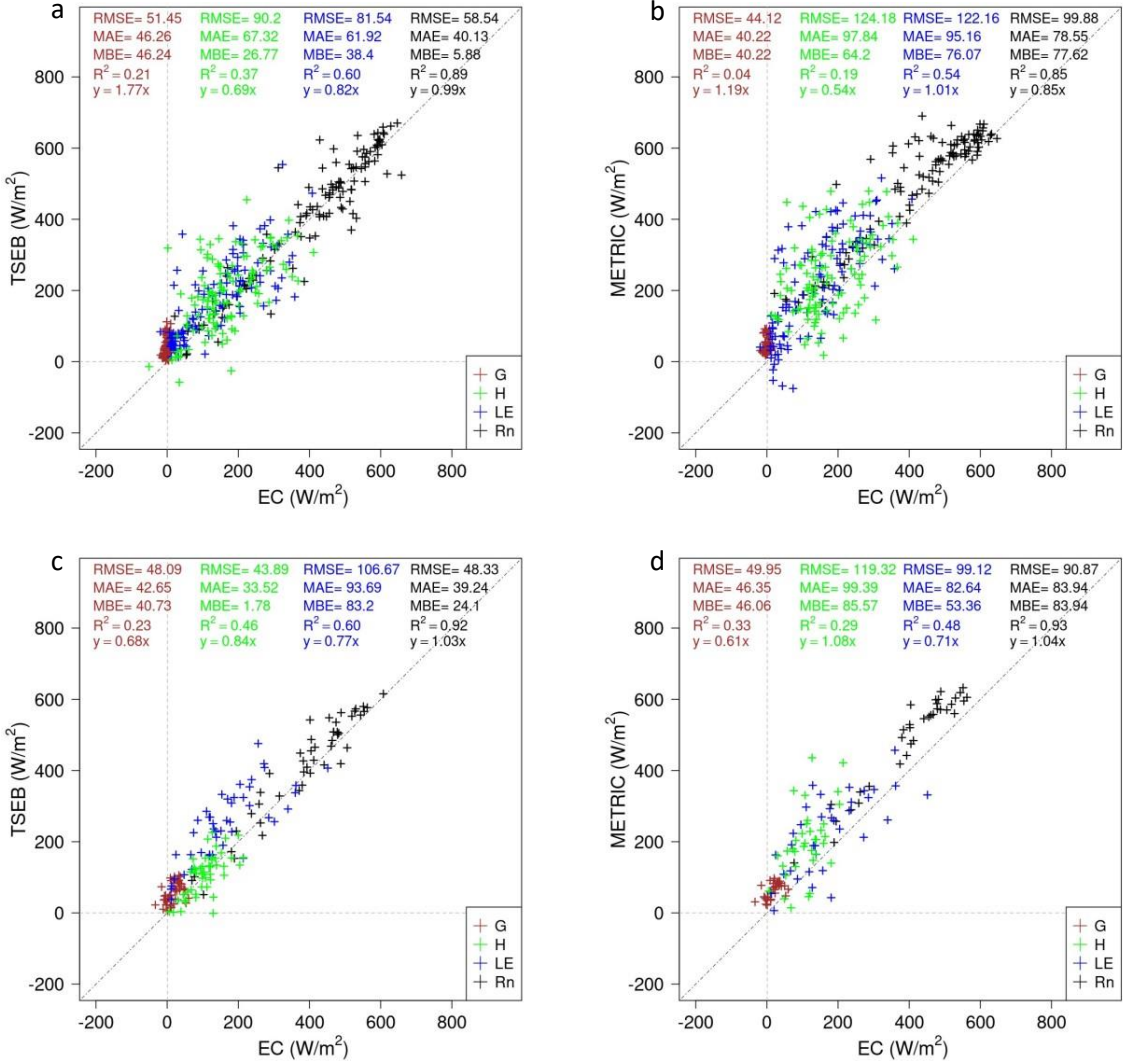


Fig. 4 Scatter plots of comparisons between the TSEB model and EC (a, c) and the METRIC model and EC (b, d) for energy fluxes (Rn, LE, H, G) in the Forest (upper images) and Grassland (bottom images) without the EBC adjustment.

The comparison of these values for the Grassland (Fig. 4 c, d) revealed good correlations between the models and the EC method. The TSEB well estimated H ( $MBE_{TSEB} = 1.78 \text{ W/m}^2$ ,  $R^2_{TSEB} = 0.46 \text{ W/m}^2$ ) but overestimated LE ( $MBE_{TSEB} = 83.20 \text{ W/m}^2$ ,  $R^2_{TSEB} = 0.60 \text{ W/m}^2$ ). The METRIC showed a performance similar to that for the Forest and overestimated H ( $MBE_{METRIC} = 85.57 \text{ W/m}^2$ ,  $R^2_{METRIC} = 0.29 \text{ W/m}^2$ ) and LE ( $MBE_{METRIC} = 53.36 \text{ W/m}^2$ ,  $R^2_{METRIC} = 0.48 \text{ W/m}^2$ ). Compared to those from both models, the measured G yields were lower at both test sites.

For the purpose of evaluating the METRIC and TSEB models, the EBC of the EC method was enforced in both comparisons using the Bowen ratio adjustment method. (Fig. 5). The results for the TSEB indicate an underestimation in H ( $MBE_{TSEB} = -35.32 \text{ W/m}^2$  and  $R^2_{TSEB} = 0.32$ ) but good agreement in LE ( $MBE_{TSEB} = -5.05 \text{ W/m}^2$  and  $R^2_{TSEB} = 0.62$ ) in the Forest (Fig. 5 a). Overall, the forced EBC showed improved agreement between the METRIC model and the EC (Fig. 5 b) compared to that of the comparison without forced EBC (Fig. 4 b). The METRIC model well estimated H, with  $MBE_{METRIC} = 3.43 \text{ W/m}^2$  and  $R^2_{METRIC} = 0.23$  (without forced EBC,  $MBE_{METRIC} = 64.20 \text{ W/m}^2$ ,  $R^2_{METRIC} = 0.19$ ) and overestimated LE, with  $MBE_{METRIC} = 33.97 \text{ W/m}^2$  with  $R^2_{METRIC} = 0.60$  (without forced EBC,  $MBE_{METRIC} = 76.07 \text{ W/m}^2$ ,  $R^2_{METRIC} = 0.54$ ). However, the METRIC model still exhibited few significant differences in H, exceeding  $200 \text{ W/m}^2$ . In the Grassland, the TSEB model underestimated H, with  $MBE_{TSEB} = -44.81 \text{ W/m}^2$  and  $R^2_{TSEB} = 0.32$ , and slightly overestimated LE, with  $MBE_{TSEB} = 28.17 \text{ W/m}^2$  and  $R^2_{TSEB} = 0.80$  (Fig. 5 c). Similarly, as in the Forest, forcing EBC of the EC improved the agreement with the METRIC model. However, the METRIC model still slightly overestimated H, with a  $MBE_{METRIC} = 37.47 \text{ W/m}^2$  and an  $R^2_{METRIC} = 0.29$  but well estimated LE, with a  $MBE_{METRIC} = 0.41 \text{ W/m}^2$  and an  $R^2_{METRIC} = 0.52$  (Fig. 5 d).

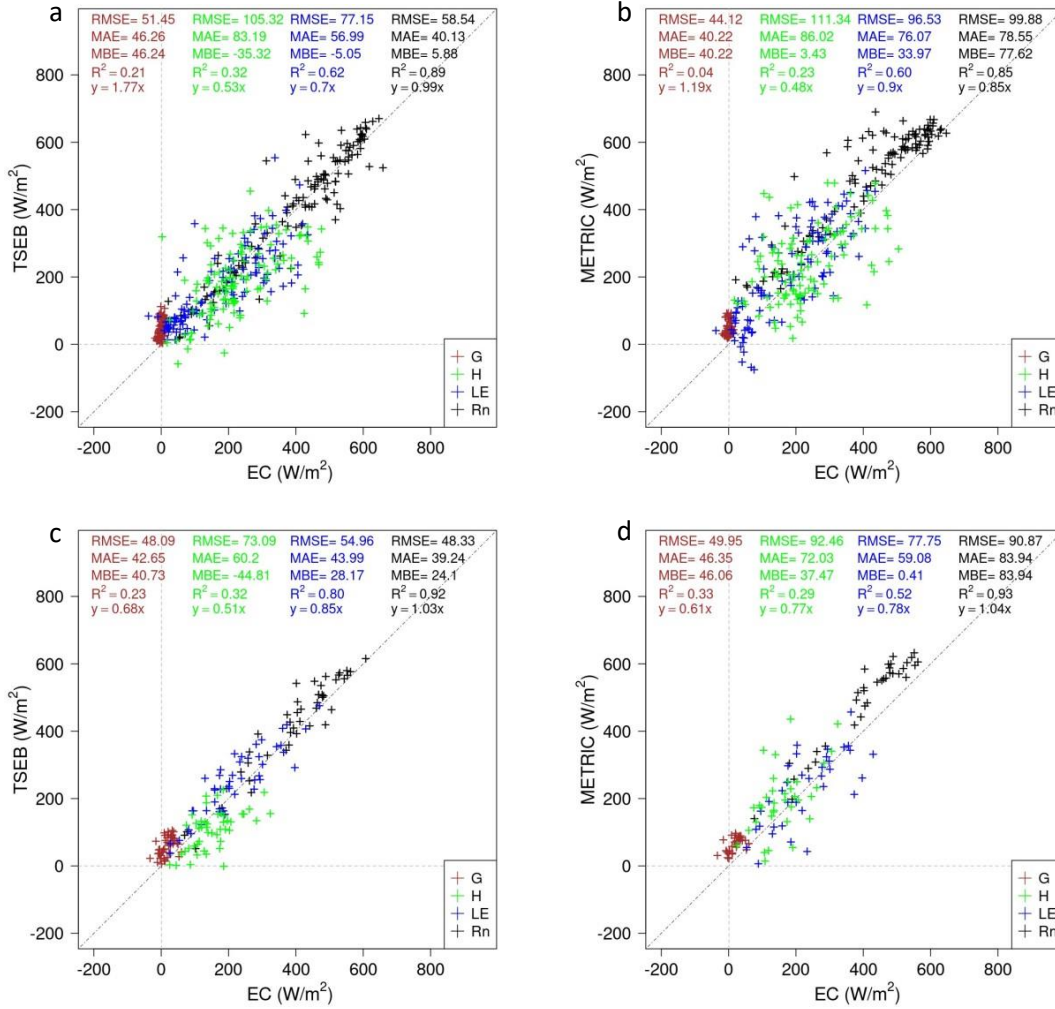


Fig. 5 Scatter plots of comparisons between the TSEB model and EC method (a, c) and the METRIC model and EC method (b, d) for energy fluxes (Rn, LE, H, G) in the Forest (upper panel) and Grassland (bottom panel) after the forced energy balance closure preserving the measured Bowen ratio (H/LE).

The instantaneous LE data from the TSEB and METRIC models were scaled to the daily ET<sub>a</sub> outputs and compared to the EC measurements without and with the EBC adjustment in Forest and Grassland. Overall, both models demonstrated satisfactory performance in estimating daily ET<sub>a</sub> values without EBC adjustment at the Forest (Fig. 6 a, b), with both models indicating MBE values close to 0 (MBE<sub>TSEB</sub> = -0.03 mm/day, MBE<sub>METRIC</sub> = 0.12 mm/day) and RMSE values lower than 1 mm (RMSE<sub>TSEB</sub> = 0.70 mm/day, RMSE<sub>METRIC</sub> = 0.86 mm/day). Although the models demonstrate good agreement with the EC method without EBC adjustment, both indicate few values where the disagreement were greater than 2 mm at the Forest. A comparison of the models to the EC method with EBC adjustment showed worse

agreement when both models underestimated the daily  $ET_a$  ( $MBE_{TSEB} = -0.5$  mm/day,  $MBE_{METRIC} = -0.39$  mm/day).

In the Grassland (Fig. 6 c, d), a comparison of the models to the EC method without EBC adjustment demonstrated slightly worse agreement for the TSEB model than for METRIC model ( $MBE_{TSEB} = 0.57$  mm/day,  $MBE_{METRIC} = -0.03$  mm/day). However, the TSEB model had improved  $R^2$  values ( $R^2_{TSEB} = 0.80$ ,  $R^2_{METRIC} = 0.62$ ) and lower RMSE values ( $RMSE_{TSEB} = 0.85$  mm/day,  $RMSE_{METRIC} = 0.90$  mm/day). The comparison of daily  $ET_a$  between the TSEB model and the EC with EBC adjustment showed improved agreement in the Grassland ( $MBE_{TSEB} = 0.1$  mm/day) but worsened in the case of the METRIC model ( $MBE_{METRIC} = -0.42$  mm/day) in the Forest.

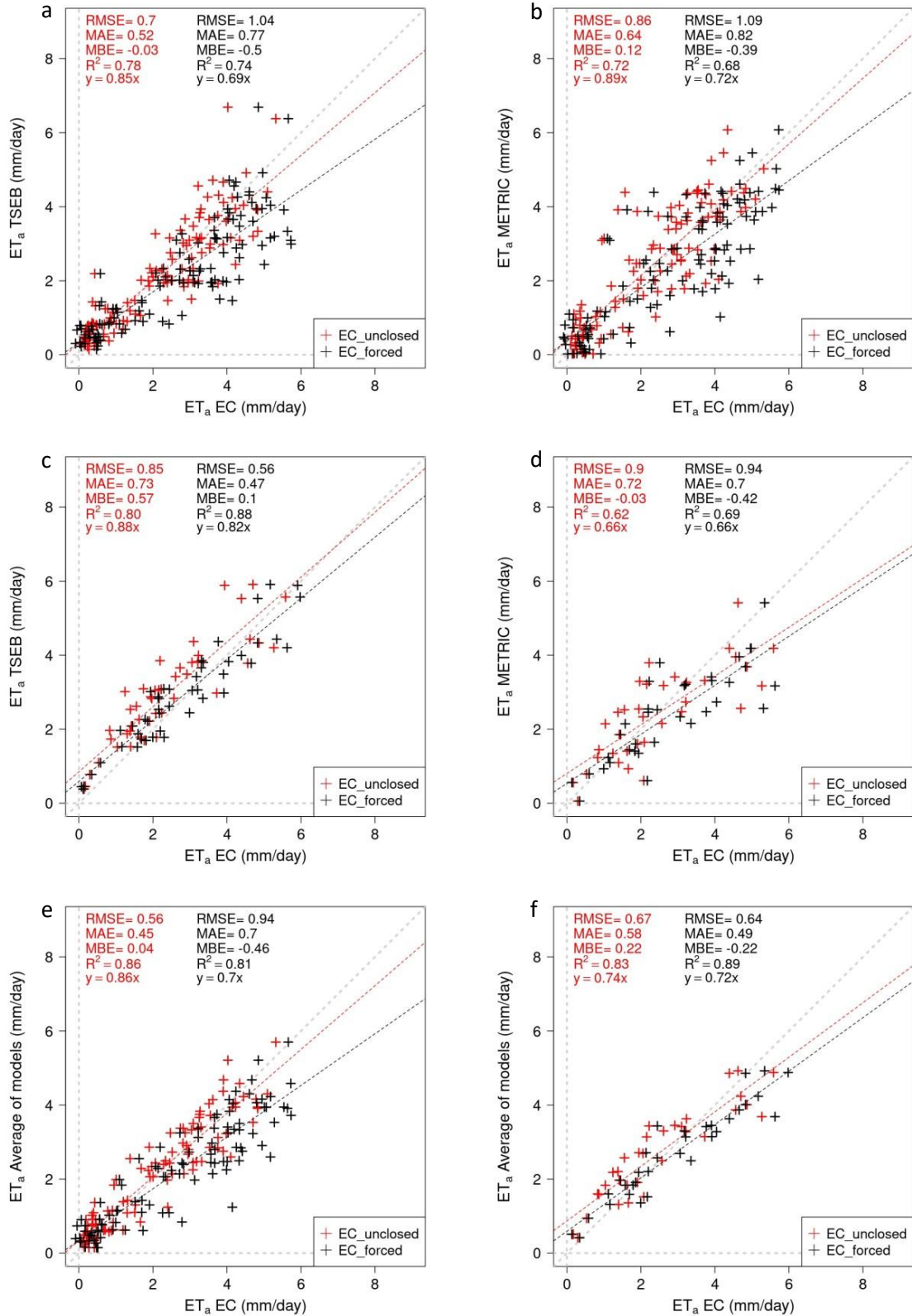


Fig. 6 Comparisons of  $ET_a$  daily values between the TSEB model and the EC method (a, c), the METRIC model and the EC method (b, d) and average of the models'  $ET_a$  values and those of the EC method (e, f) in the Forest (a, b, e) and Grassland (c, d, f). Red points depict model comparisons with the EC method

without EBC adjustment (EC\_unclosed), while black points represent comparisons with EBC adjustment (EC\_forced).

Because both models often indicate opposite bias compared to EC, the daily  $ET_a$  values of both models were averaged and compared to those of the EC method with and without EBC adjustment in the Forest (Fig. 6 e) and Grassland (Fig. 6 f). Compared to the agreement between the TSEB model and the EC method (Fig. 6 a) and between the METRIC model and the EC method (Fig. 6 b) in the Forest, the comparison of averages to EC method values without EBC adjustment (Fig. 6 e) demonstrated improved agreement in all the metrics except for the MBE, where a similar value (0.04 mm/day) was detected as in the case of the TSEB model and EC method (-0.03 mm/day). The same pattern was detected for the comparison of the model averages to EC method values with EBC adjustment, where averages indicated a worse MBE (-0.46 mm/day) than in the METRIC-EC comparison ( $MBE_{METRIC} = -0.39$  mm/day).

In the case of Grassland (Fig. 6 f), the comparison of averaged model values showed improved agreement with that of EC values without EBC adjustment, except for MBE, which was 0.22 for average values and 0.03 for the METRIC model and EC method (Fig. 6 d). Comparison of averages to EC values with EBC adjustment slightly worsened the agreement in error metrics compared to the TSEB – EC comparison (Fig. 6 c) in most metrics but improved agreement with the METRIC – EC comparison (Fig. 6 d) in all metrics.

### **4.3 Intercomparison of the METRIC and TSEB models**

Intercomparison between the TSEB and METRIC models was conducted within 99 common outputs. In the Forest (Fig. 7 a), a comparison of H indicated generally lower H ( $y = 0.26x$ ) and LE ( $y = 0.5x$ ) values in the TSEB model. Both models also demonstrated similar G values, where the TSEB model yielded slightly lower outputs than did the METRIC model ( $y = 0.83x$ ) and different estimates of  $R_n$  for some outputs. In the Grassland (Fig. 7 b), the TSEB model showed lower  $R_n$  values and a significantly lower H ( $y = 0.37x$ ) than did the METRIC model. Nevertheless, there was slightly improved agreement in the LE ( $R^2 = 0.45$ ,  $y = 0.73x$ ).

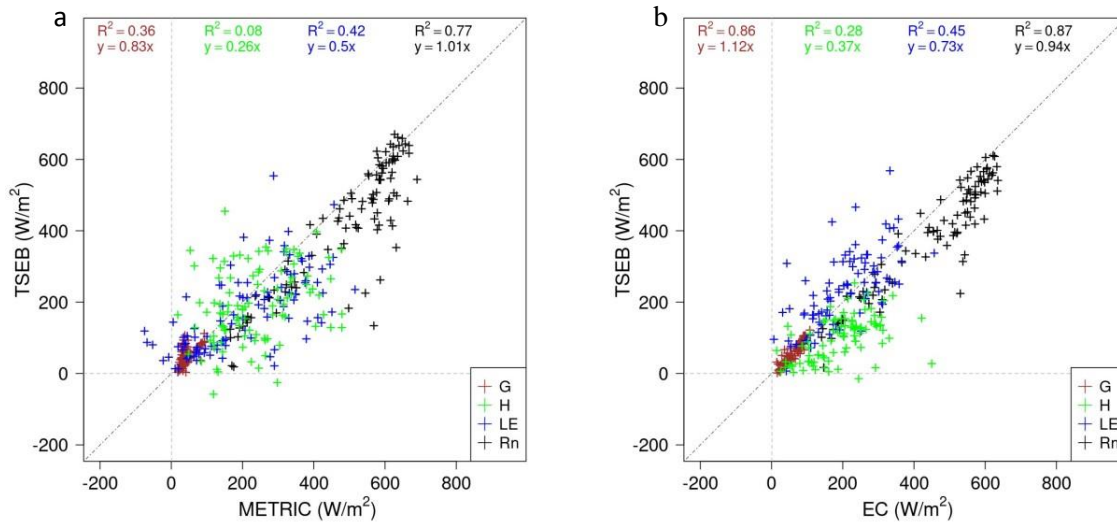


Fig. 7 Scatter plots of comparisons of energy flux values (Rn, LE, H, G) between the TSEB and METRIC models in the Forest (a) and Grassland (b) in the period 2015–2021.

Both models and the EC method without EBC adjustment captured the seasonal variability in H throughout the year (Fig. 8). The highest H values varied between years in the Forest (Fig. 8 a); however, most H values occurred in the first half of the growing season (April–May) when the surface was not fully covered by vegetation. The greatest average values at the time of satellite overpass were indicated by the METRIC model (237.28 W/m<sup>2</sup>) compared to those from the TSEB model (194.70 W/m<sup>2</sup>) and EC method (171.28 W/m<sup>2</sup>) in the Forest. The METRIC model also showed the highest instantaneous H value on March 20, 2021 (479.16 W/m<sup>2</sup>), while the TSEB showed the maximal H value on July 10, 2021 (454.83 W/m<sup>2</sup>), and the EC method showed it on April 16, 2016 (411.21 W/m<sup>2</sup>). Both models and the EC method also indicated similar variabilities ( $\sigma_{\text{TSEB}} = 104.34 \text{ W/m}^2$ ,  $\sigma_{\text{METRIC}} = 110.80 \text{ W/m}^2$ ,  $\sigma_{\text{EC}} = 88.60 \text{ W/m}^2$ ). A relatively high discrepancy between the models and the EC was shown in the summer of 2019 and in the second part of 2021, where both models consistently overestimate H. Compared with the TSEB model and the EC, the METRIC model also evidently indicated higher values in the summer of 2015. A similar pattern was detected in the Grassland compared to the Forest (Fig. 8 b), where the METRIC consistently indicated greater H values than did the TSEB and EC. This was confirmed by average instantaneous values at the satellite overpass, where good agreement was detected between the TSEB model (100.14 W/m<sup>2</sup>) and the EC method (109.79 W/m<sup>2</sup>), while the METRIC model indicated a

higher H value ( $193.57 \text{ W/m}^2$ ). The highest maximal H value was detected by the METRIC model on March 20, 2015 ( $449.72 \text{ W/m}^2$ ).

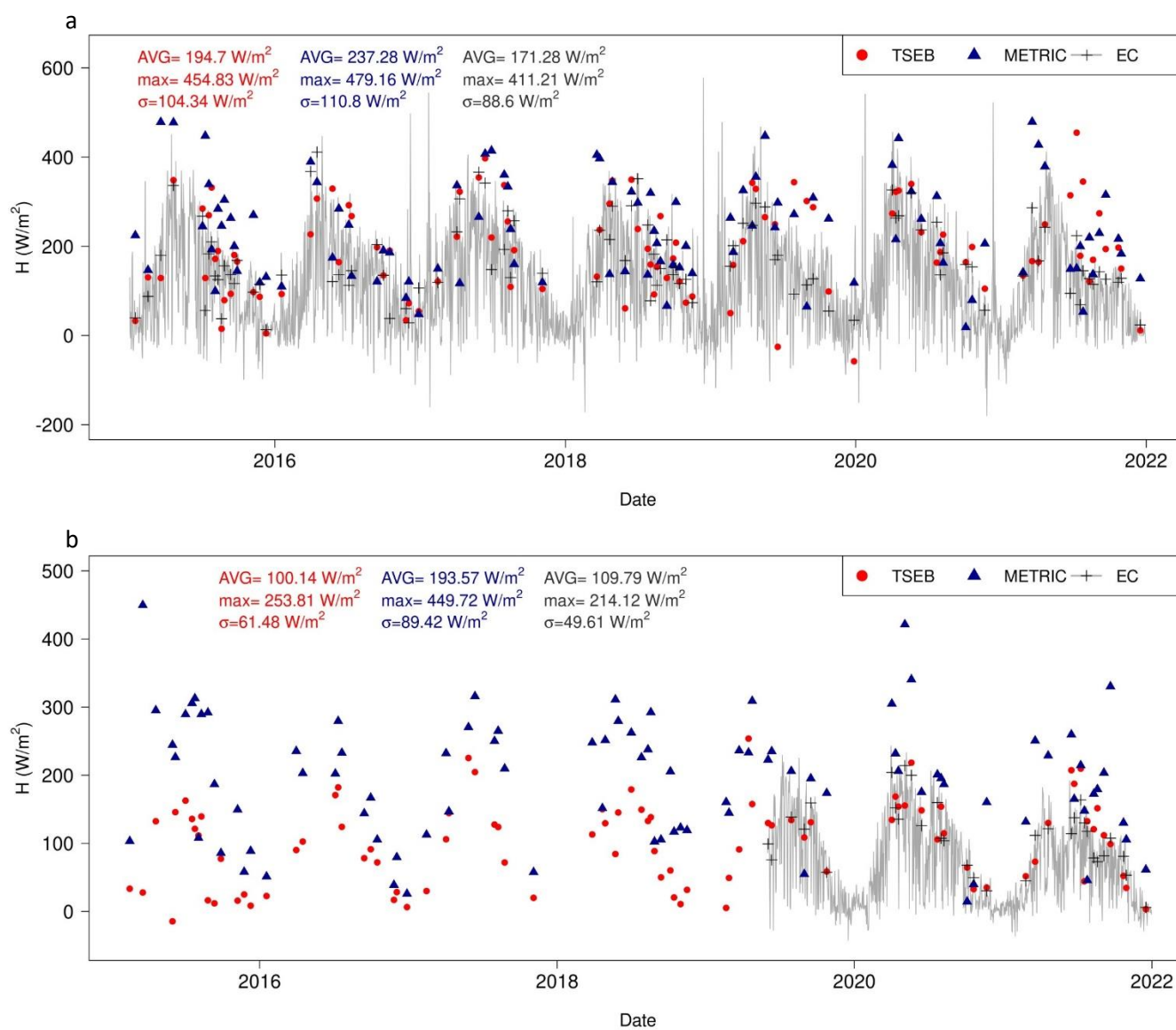


Fig. 8 Temporal variation of H data from the TSEB and METRIC models in the period 2015–2021 at time of satellite overpass in Forest (a) and Grassland (b). The gray line depicts daily EC values while the black crosses depict instantaneous EC data. The AVG show average daily values, max mean maximal daily measured values and  $\sigma$  mean standard deviation value.

In the case of the  $ET_a$  model intercomparison (Fig. 9), a relatively high disagreement was detected between the TSEB and METRIC models in the Forest ( $R^2 = 0.56$ ,  $y = 0.68x$ ). The results were more consistent for Grassland ( $R^2 = 0.61$ ); however, it was also evident that the TSEB model shows higher values than the METRIC model.

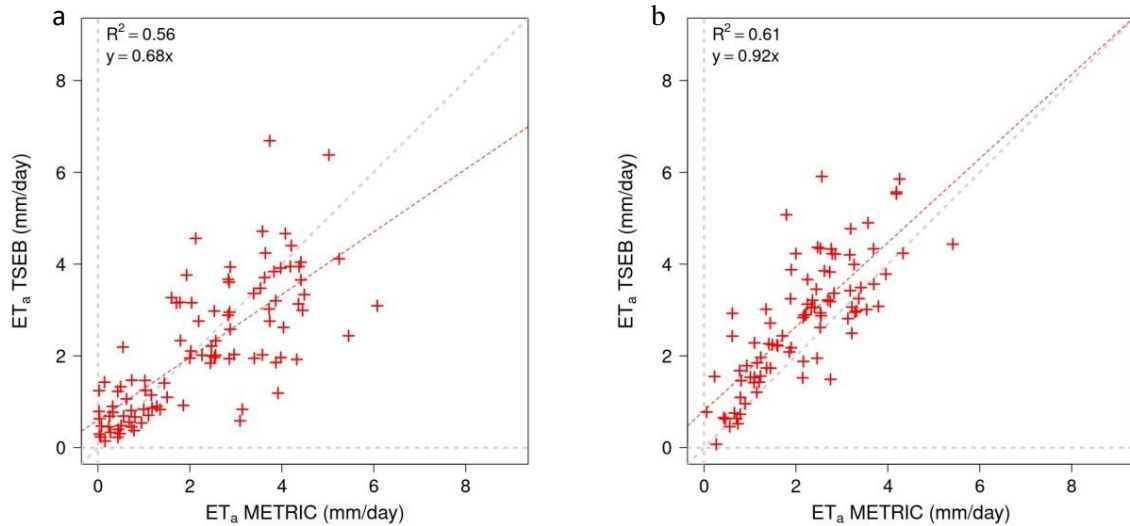


Fig. 9 Comparisons of  $ET_a$  daily values between the TSEB and METRIC models in Forest (a) and Grassland (b) in the period 2015–2021.

Both models were able to capture seasonal variability during the years (Fig. 10). The average daily  $ET_a$  values between the models and the EC without EBC adjustment were similar ( $AVG_{TSEB} = 2.1$  mm/day,  $AVG_{METRIC} = 2.3$  mm/day,  $AVG_{EC} = 2.2$  mm/day) in the Forest (Fig. 10 b). The METRIC model outputs revealed the greatest variability; however, the values of variability were almost identical between the models and the EC method ( $\sigma_{TSEB} = 1.4$  mm/day,  $\sigma_{METRIC} = 1.6$  mm/day,  $\sigma_{EC} = 1.7$  mm/day). A maximum daily value of 6.7 mm was recorded by the TSEB model on June 19, 2019, while in the METRIC model this value reached 6.08 mm on July 26, 2021. These two values were approximately 2 mm greater than the maximal value detected by the EC method (4.1 mm/day) among the available clear-sky satellite images. The highest discrepancy between the two models was detected on June 19, 2019, when the TSEB model exhibited a higher value of approximately 3.0 mm/day. In the Grassland (Fig. 10 b), the TSEB model had the highest daily  $ET_a$  average (2.8 mm/day) compared to those of the EC method (2.5 mm/day) and the METRIC models (2.1 mm/day). The TSEB model exhibited similar  $ET_a$  variability to that of the EC method ( $\sigma_{TSEB} = 1.3$  mm/day,  $\sigma_{EC} = 1.5$  mm/day) but greater than that of the METRIC

model ( $\sigma_{\text{METRIC}} = 1.1 \text{ mm/day}$ ). The maximal value for the TSEB model (5.9 mm/day) was observed on June 12, whereas the METRIC model recorded the maximal  $\text{ET}_a$  on July 26, 2021 (5.4 mm/day). Higher values of  $\text{ET}_a$  were detected in the last monitored year (2021). These higher values corresponded to the detected H (Figure 8 b), which indicated lower H during that year in the Grassland.

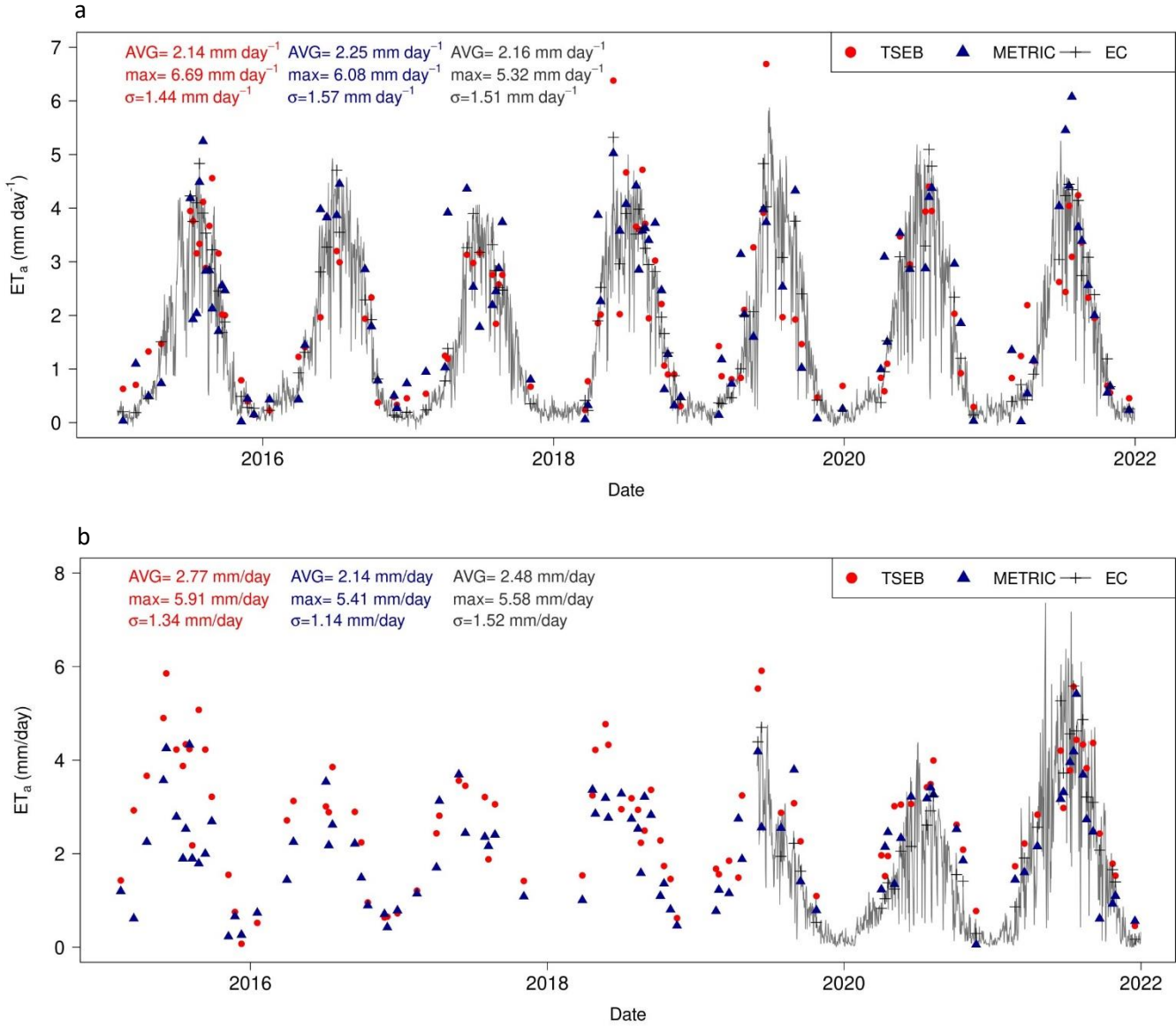


Fig. 10 Temporal variation of  $\text{ET}_a$  daily data of the TSEB and METRIC models during the period 2015–2021 in the Forest (a) and Grassland (b). The gray line represents all available EC daily  $\text{ET}_a$ , while the black crosses depict EC daily  $\text{ET}_a$  data for the days of model outputs.

#### 4.4 Instantaneous evaporative fraction and Bowen ratio

Both models and the EC method without EBC adjustment were utilized to calculate the evaporative fraction and Bowen ratio. The evaporative fraction expresses how much available energy ( $R_n-G$ ) is partitioned into LE, i.e.,  $LE/(R_n-G)$ . In the Forest plots (Fig. 11 a), the median values ranged between 0.3 and 0.6 for both models during the growing season. The lowest median for both models and the EC method was detected in April ( $\text{median}_{\text{METRIC}}= 0.33$ ,  $\text{median}_{\text{TSEB}}= 0.29$ ,  $\text{median}_{\text{EC}} = 0.14$ ). The highest median was detected in August for both models (0.60 for METRIC and TSEB) and in July for the EC method (0.49). Both models and the EC method also exhibited increasing trends during the spring–summer period and decreasing trends in August (July)–September. These trends can indicate seasonal characteristics, where available energy was mostly partitioned into LE in summer and less during the start and end of a growing period. The interquartile ranges detected by the models mostly varied between 0.2 and 0.8 and exhibited a relatively large range during single months. The highest interquartile range was detected in April for the METRIC model (0.31, between 0.23 and 0.54) and in August for the TSEB model (0.23, between 0.50 and 0.73). The EC method indicates lower interquartile ranges than the models with a maximum in August (0.18).

In the Grassland (Fig. 11 b), while the median range from the TSEB model was typically between 0.5 and 0.8, the median range from the METRIC model mostly falls between 0.4 and 0.7. The highest median values were observed in September for the TSEB model (0.77) and in June for the METRIC model (0.66) and EC method (0.56). The lowest medians were found in May for both models ( $\text{median}_{\text{TSEB}} 0.59$ ,  $\text{median}_{\text{METRIC}} = 0.43$ ) and in April for EC (0.21). Moreover, the TSEB model exhibited an increasing trend between May and September, and compared with the METRIC model and EC method, the TSEB model exhibited lower differences between spring and summer period. The TSEB model estimates that the available energy was more efficiently utilized for LE during the latter part of the growing season. The interquartile range was widest in June for the TSEB model (0.19, ranging from 0.58 to 0.77), in August for the METRIC model (0.24, ranging from 0.41 to 0.65) and in July for the EC method (0.33 between 0.38 and 0.71).

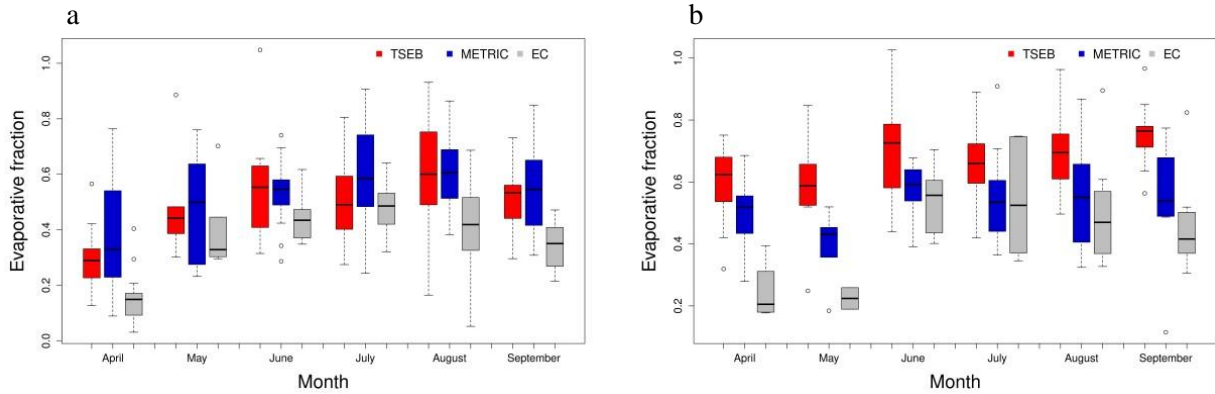


Fig. 11 Boxplots show monthly evaporative fraction data of the TSEB (red) and METRIC (blue) models supplemented by the EC method (gray) in the growing season in the Forest (a) and Grassland (b). The range of the boxplots express daily values within months.

The Bowen ratio describes the ratio between  $H$  and  $LE$ , i.e.,  $H/LE$ . The highest medians were detected in April (2.03, 2.47 and 4.00 for the METRIC, TSEB and EC, respectively) in the Forest (Fig. 12 a). The lowest median was detected in August for both models and for the EC method (0.65, 0.67 and 0.64 for the METRIC, TSEB and EC, respectively). The detected median values of the models and EC also indicate a trend during the growing season when the Bowen ratio decreases in spring, with lower values occurring in summer and September. This trend indicates that the available energy was more utilized for  $LE$  in the second part of the growing season, whereas  $H$  was predominant in the first part of the season. This pattern corresponds to the temporal variation in  $H$  (Fig. 8 a). The greatest interquartile range was displayed in April (for the METRIC model, 2.51; 0.85-3.36; for the TSEB model, 1.34; 2.04-3.38; and for the EC method, 2.42; 5.48-3.05).

In the Grassland (Fig. 12 b), most of the median values detected by the models were less than 1 except in May for the METRIC (1.32). A value less than 1 indicates that more available energy at the surface was partitioned into  $LE$  in the Grassland. The median value from the EC was greater than 1 in April (1.80) and May (2.00). The highest median for both models was detected in May (for TSEB, 0.70; for the METRIC, 1.32). Both models indicate relatively well a decreasing trend during the growing season, when maximal medians were displayed during spring and minimal medians in summer (for the TSEB,

in September 0.31, for the METRIC, in June 0.69, and for EC in June 0.36). While the METRIC model exhibited a greater interquartile range in most months than did the TSEB model during the growing season, the highest interquartile range was observed for the EC in April (1.56). The TSEB model exhibited the maximum interquartile range in June (0.42), while the METRIC had the highest value in August (0.91).

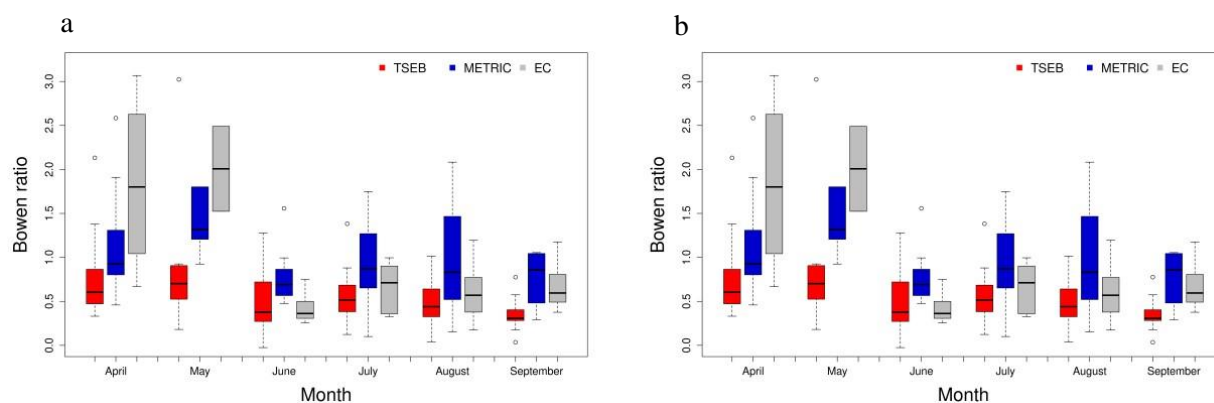


Fig. 12 Boxplots show monthly Bowen ratio data of the TSEB (red) and METRIC (blue) models supplemented by the EC (gray) in the growing season in the Forest (a) and Grassland (b). The range of the boxplots express daily values within months.

#### 4.5 Example of spatial outputs

While the footprints of the EC systems mostly capture a homogenous land surface, both stations are surrounded by different ecosystems; therefore, there is an opportunity to identify spatial differences in the distributions of model outputs (daily  $ET_a$ , H, LE) and other variables (LST, LAI). The chosen image series of two selected days (Figs. 13, 14) represents some of the disagreements between the models in forested and grassed areas. In the first case (Fig. 13), the LST ranged between 295 K and 305 K, with high LAI values of approximately 5 in the Forest. In these conditions, the TSEB model yielded higher H values of approximately 110 W/m<sup>2</sup>, lower LE values of approximately 130 W/m<sup>2</sup>, and lower  $ET_a$  values of approximately 1 mm/day than the METRIC model at the Forest.

Differences between the models were shown for the Grassland. The LST was greater in the Grassland (approximately 310 K) than in the surrounding forests, where the temperature varied by approximately 300 K. Additionally, a significantly lower LAI of approximately 1 was detected in the Grassland compared to the forest area around (LAI = 5).

The TSEB model indicated a similar  $ET_a$  (4.0 mm/day) as the EC without EBC adjustment (3.9 mm/day) in the Grassland, which was not included in the image series (Fig. 13). The METRIC model indicated lower  $ET_a$  (2.2 mm/day). The results demonstrated that the TSEB model estimated  $ET_a$  relatively well despite its low LAI (approximately 1). A significant disparity between the TSEB and METRIC models became evident in the surrounding areas near the Grassland, where the forested area was mostly located, and where both models indicated opposing patterns. In these areas, the TSEB model had significantly greater H and markedly lower LE and  $ET_a$  than the METRIC model. This disagreement between the models could be caused by the reduction in the  $\alpha$  coefficient in the TSEB model, which was significantly greater in the grassed areas than in the forested areas, thus strongly reducing  $ET_a$  in the forest in this case. For this reason, the TSEB model results do not seem to correlate with high LSTs, which are greater in grassed areas than in forests. The comparison of the models and the EC method without EBC adjustment outputs also showed relatively unexpected results between the Forest and Grassland test sites. Despite the greater difference in LAI among the Forest (approximately 5) and Grassland (approximately 1), the difference was relatively low in  $ET_a$ . The EC method indicated a lower  $ET_a$  of approximately 1.5 mm/day, and the TSEB model indicated a lower  $ET_a$  of approximately 1 mm/day in Grassland than in Forest stations.

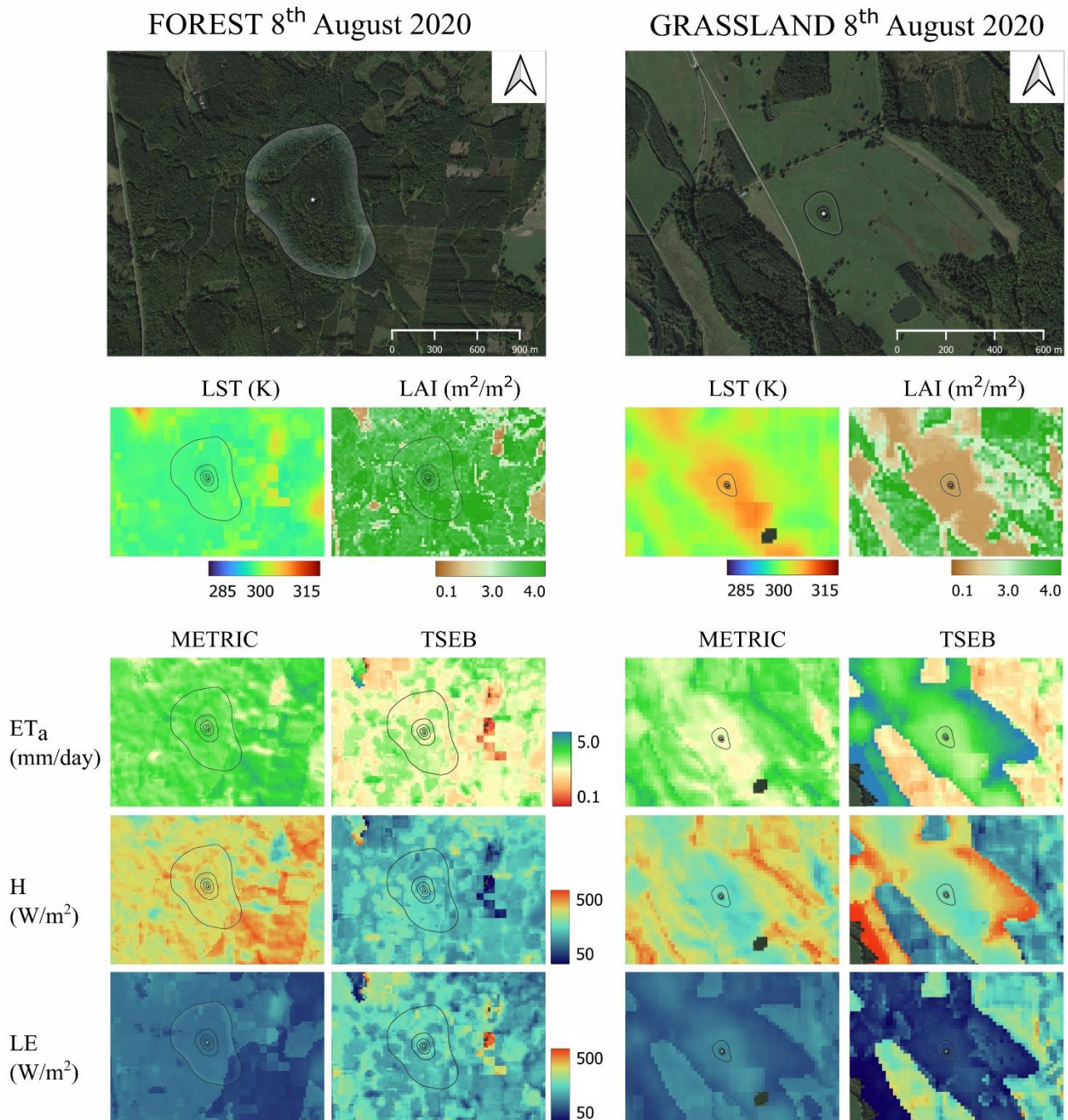


Fig. 13 Map outputs illustrating the spatial distribution of selected variables (LST, LAI) and the outputs (daily  $ET_a$ , H, and LE) of the TSEB and METRIC models in Forest and Grassland for 20th August 2020.

The second image series showed map outputs of instantaneous values and daily  $ET_a$  values from September 5th, 2021 (Fig. 14). The LST results indicated an LST of approximately 295 K and a high LAI of approximately 5 at the Forest. The results of the models indicated good agreement among themselves at this site (the TSEB model estimated  $ET_a = 2.27$  mm/day,  $LE = 187$  W/m<sup>2</sup>,  $H = 264$  W/m<sup>2</sup>; the METRIC model estimated  $ET_a = 2.56$  mm/day,  $H = 230$  W/m<sup>2</sup>,  $LE = 245$  W/m<sup>2</sup>). Compared to that

in the Forest site, the LST in the Grassland was greater (LST = 305 K) but was similar in the surrounding forested areas around the Grassland station. The LAI was lower in the Grassland (LAI = 2.5 – 3) than in forested areas (LAI $\approx$ 5).

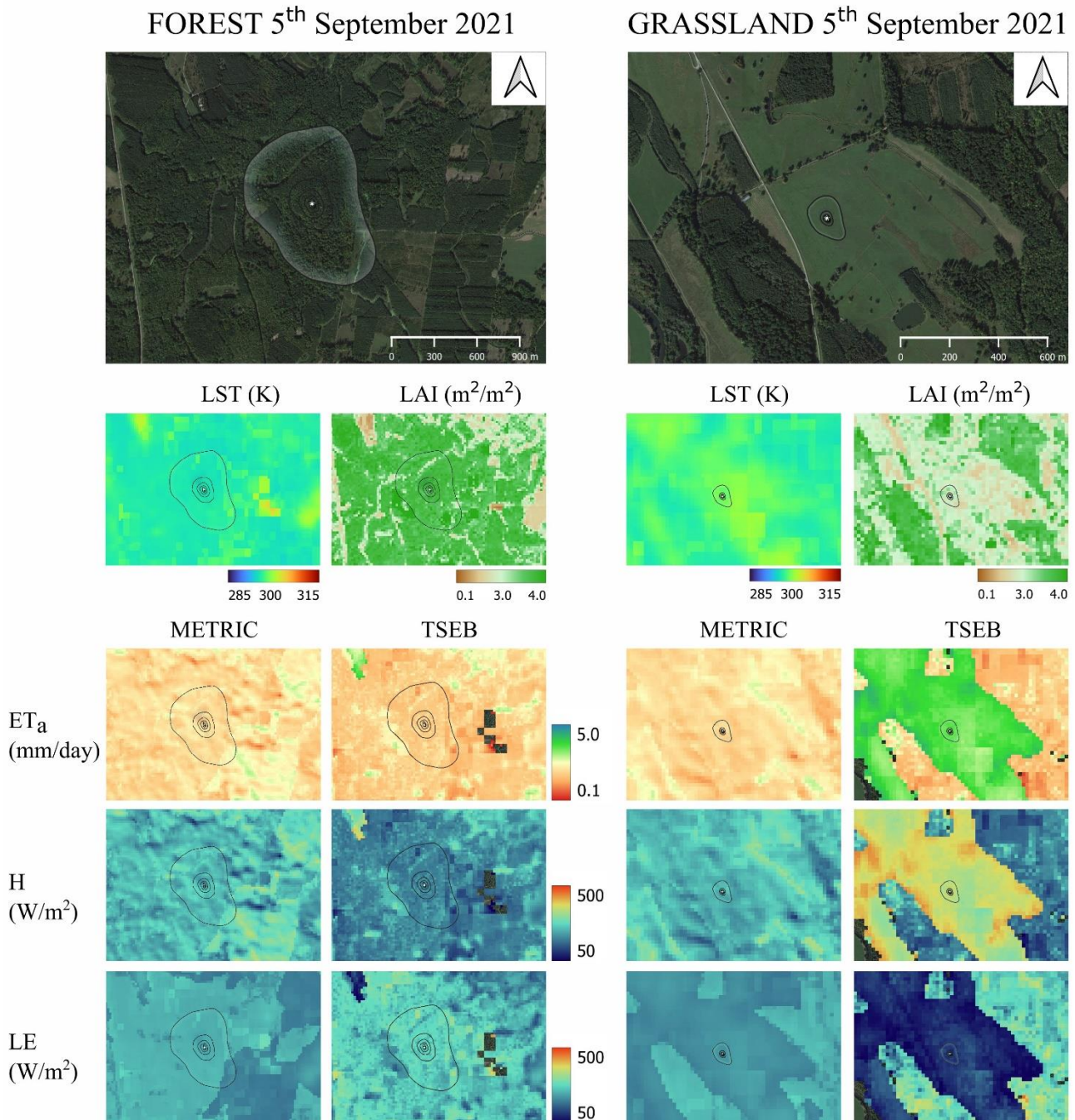


Fig. 14 Map outputs illustrating the spatial distribution of selected variables (LST, LAI) and the outputs (daily  $ET_a$ , H, and LE) of the TSEB and METRIC models in Forest and Grassland for 5th September 2021.

Both models indicated disagreement in terms of energy fluxes and daily  $ET_a$  in the Grassland where the TSEB model calculated a lower  $H$  of approximately  $100 \text{ W/m}^2$  than the METRIC model and therefore calculated a higher  $LE$  of approximately  $130 \text{ W/m}^2$  and an  $ET_a$  of approximately  $2 \text{ mm/day}$ . In contrast to those of the METRIC model, the TSEB values also differed greatly between the Grassland and surrounding forest area. The spatially oriented outputs of the TSEB model cannot fully correlate with the LST, which was greater in the Grassland than in the surrounding forested area. Like in Fig. 13, this disagreement could be caused by a decrease in the a priori  $\alpha$  coefficient in the forested areas.

The results of the EC method without EBC adjustment yielded  $3.1 \text{ mm/day}$  for the Forest and  $3.1 \text{ mm/day}$  for the Grassland, demonstrating that METRIC ( $2.6 \text{ mm/day}$  and  $2.4 \text{ mm/day}$ ) more accurately represented  $ET_a$  than TSEB ( $2.3 \text{ mm/day}$  and  $4.4 \text{ mm/day}$ ) in the Forest and Grassland on this date. A similar pattern between  $ET_a$  and the LAI, as shown in Fig. 13, was detected between the Forest and Grassland test sites. While the outputs of the LAI demonstrated a significant difference (Forest = 5, Grassland = 2.5), the  $ET_a$  values were similar in the Grassland and Forest as detected by the METRIC and EC, and even greater in the Grassland as indicated by the TSEB.

#### **4.9 Monthly and annual results of $ET_a$**

An interpolated  $ET_a$  values from the TSEB and METRIC models supplemented by EC measurements without and with EBC adjustment demonstrated annual values of  $ET_a$  in the monitored years at both sites for EC (Fig. 15). Annual values detected by models mostly vary between  $400$  and  $600 \text{ mm/year}$  in the Forest. The highest annual  $ET_a$  value detected by models ( $632 \text{ mm}$ ) was calculated in 2016 for the METRIC outputs, while the TSEB and EC values were  $504 \text{ mm}$  and  $556 \text{ mm}$ , respectively, for the same year. Greater agreement between models and EC daily measurements was observed for EC without EBC compared to EC with EBC adjustment, where values were consistently greater in the Forest. At the Grassland, the calculated values of the TSEB model were consistently greater than those of the METRIC model and EC method. This pattern corresponds to other results (Figs. 9 b, 10 b) where TSEB mostly overestimate daily  $ET_a$  values compared to METRIC model. The highest annual  $ET_a$  value detected by models ( $722 \text{ mm}$ ) was calculated in 2019 for the TSEB, while the METRIC data had values of  $527 \text{ mm}$  and  $542 \text{ mm}$ , respectively, for the same year. The greatest difference between TSEB and EC

values were detected in 2020, with a deviation of 200 mm, while the largest difference between the METRIC and EC values was observed in 2021, when the METRIC model indicated lower values of approximately 187 mm. The annual results from the EC method also showed larger differences in  $ET_a$  between 2020 and 2021. However, the EC value was only 427 mm in 2020 and 715 mm in 2021.

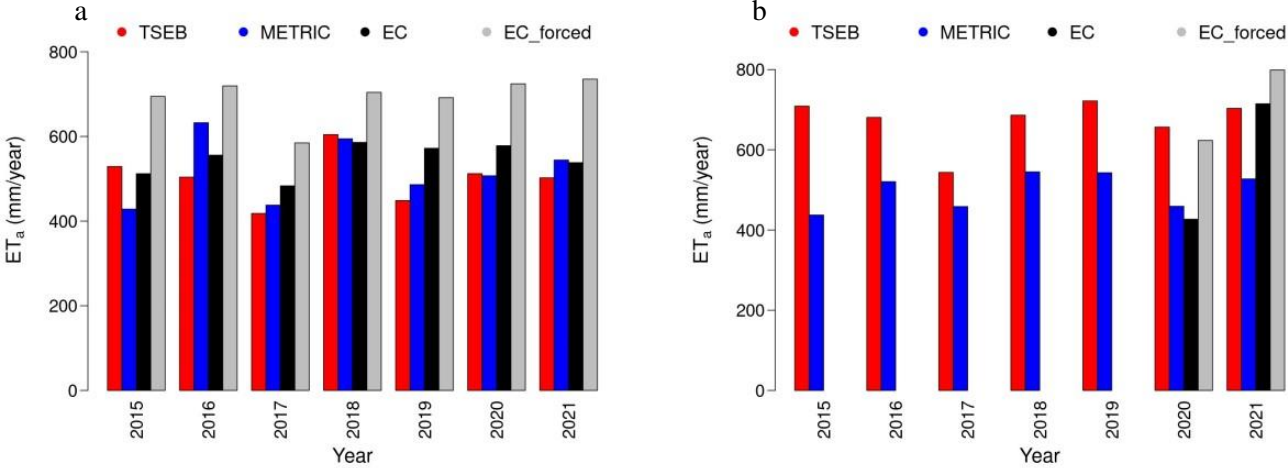


Fig. 15 Annually (a, b) interpolated daily  $ET_a$  values calculated from the TSEB (red columns) and METRIC (blue columns) models and the EC method without EBC (black columns) and with EBC adjustment (gray columns) in the Forest (left) and Grassland (right).

## 5 Discussion

The main goal of this study was to evaluate the METRIC and TSEB remote sensing models at two test sites representing different contrasting land covers in the unique hydrological floodplain area of southern Moravia in the Czech Republic. Both models demonstrated the ability to quantify  $ET_a$  at both test sites, thereby illustrating the considerable potential of remote sensing methods and models for the precise quantification of the hydrological balance under conditions in Central Europe.

An important aspect of the study involves the comparison of daily  $ET_a$  outputs between models and the EC. Both methods showed good agreement with the EC without EBC adjustment in concordance with the findings of other studies, which generally showed good agreement between the models (Choi et al., 2009; French, Hunsaker and Thorp, 2015; Peddinti and Kisekka, 2022). However, both methods presented opposite bias in the Forest and Grassland. TSEB model demonstrated superior performance at the Forest, while the METRIC model excelled at the Grassland. The opposite trend in  $ET_a$  was evident in the intercomparison, where the TSEB model indicated lower values in the Forest and higher values in the Grassland. For this reason, the daily  $ET_a$  outputs from the METRIC and TSEB models were averaged, and the values were compared to the EC measurements. The results demonstrated improved agreement with the EC method compared to that of the individual models in the forested and grassland areas. Consequently, in focused studies on hydrological balance, it is also possible to use the average  $ET_a$  values from both evaluated models instead of the outputs from individual models.

The challenge for accurate determination of  $ET_a$  using the demonstrated method of estimating energy fluxes ( $R_n$ ,  $G$ ,  $H$ ,  $LE$ ) on the surface lies in their proper quantification. Many of the studies evaluated the METRIC or TSEB models over different land cover areas and indicated good agreement between *in situ* measurements and models (Kustas et al., 2004; Allen et al., 2007b; Timmermans et al., 2007; Choi et al., 2009). Our study also demonstrated good agreement between both models and the EC method in terms of the energy fluxes even though the TSEB model demonstrated slightly better agreement than the METRIC model, which mostly overestimated the energy fluxes at both test sites. Both models also demonstrated higher values at both sites than did the measured  $G$ . The lower  $G$  values were caused by the delayed response of the soil to the increasing energy input during the morning hours at the time of

satellite overpass. To avoid disagreements between the models and measurements, the measured  $G$  values could be potentially multiplied by the empirical coefficient 1.3 – 1.6 (Fischer et al., 2018; Pozníková et al., 2018). In this work, the  $G$  values were not multiplied by any coefficient because the values of  $G$  constitute a negligible part of the presented overall energy balance. Similarly, as in other studies (Twine et al., 2000; Choi et al., 2009; Foken et al., 2017; Fischer et al., 2018), we enforced the EBC of EC energy flux values by applying the Bowen ratio adjustment, as a significant amount of energy residue was detected at both EC sites (38% in the Forest and 30% in the Grassland). The outputs of energy fluxes, whether within a closed or un-closed energy balance, likely include actual turbulent fluxes from the tower footprint of the EC and serve as an indicator of observational uncertainty (Choi et al., 2009). While adjustment of the EBC improved the agreement for instantaneous LE between the METRIC and TSEB models and the EC method at both test sites, in the case of daily energy fluxes and thus  $ET_a$ , EBC adjustment improved agreement only for the TSEB model in the Grassland. The estimation of daily values from instantaneous values measured at satellite overpasses is one of the crucial parts of the precise calculation of  $ET_a$ . A similar underestimation of approximately 5 – 10% occurred in other studies that assessed daily  $ET_a$  (Gurney and Hsu, 1990; Sugita and Brutsaert, 1991; Brutsaert and Sugita 1992). In this study, we use different scaling methods for both models. In the case of the TSEB model, scaling assumes that the ratio between LE and solar radiation measured during satellite overpasses is constant, while for the METRIC model, the principle assumes that the ratio between  $ET_a$  and  $ET_o$  is constant. However, overall, these are still estimates of daily fluxes, and neither method fully captures the true relationships between variables. For this reason, daily  $ET_a$  values may be underestimated even though instantaneous LE values were overestimated during satellite overpasses, as shown in our results. Therefore, scaling values from instantaneous to daily values requires attention in future studies.

The process of identifying cold and hot pixels is sensitive during the METRIC model implementation (Choragudi 2011; Bhattarai et al., 2017). This requires precise detection and depends on the method used for selecting anchor pixels or even searching for the most suitable hot and cold pixels in the area of interest (Long and Singh 2013; Morton 2013). In this study, an automatic selection of the endpoints

described in Olmedo et al., (2016) was used. The selection of endpoints is identified as one of the weaknesses of the METRIC model; however, it can be relatively tolerant when certain surface data are lacking, such as biophysical parameters of vegetation. The TSEB model is more sensitive to uncertainties in LST and air temperature (Anderson et al., 1997) and requires more detailed biophysical parameters to calculate the energy balance; however, such parameters cannot be easily determined, as in the METRIC model (Chirouze et al., 2014; French, Hunsaker and Thorp, 2015; Peddinti and Kisekka, 2022). The TSEB model incorporates detailed radiative and flux exchange data between soil and vegetation components without requiring cold or hot pixels (Kustas and Norman, 1999). In contrast, the single-source models, METRIC and SEBAL, depend more on proxies such as LSTs or vegetation indices to identify wet or dry conditions in the area of interest (Bastiaanssen et al., 1998; Allen et al., 2007a). One advantage of the TSEB model is the partitioning of available energy into vegetation and soil, which allows the separation of soil evaporation from canopy transpiration (Norman et al., 1995). However, transpiration and evaporation partitioning in the TSEB model was beyond the scope of this study.

In addition to direct evaluation via charts and scatter plots, spatially distributed LST and LAI data and model outputs ( $H$ ,  $LE$ , and  $ET_a$ ) were shown in this study. Two image series of selected days were chosen because they indicate some of the disagreements between models. The series of images from 2020 can support a suggestion about the disagreement of models in sparse vegetation cover with low LAI (Choi et al., 2009; French, Hunsaker and Thorp, 2015) because the TSEB model indicates strongly greater  $ET_a$  than the METRIC model on this day in the Grassland. However, despite the low LAI of approximately 1, EC without EBC adjustment indicates a slightly lower daily  $ET_a$  than TSEB and demonstrates that the TSEB model estimated  $ET_a$  relatively well, while the METRIC model underestimated  $ET_a$ . In addition, the models and EC method effectively highlighted some inadequately confirmed hypotheses captured in two selected series of images. For the first point, the outputs from the EC method and the TSEB model suggest that vegetation, such as grassland, with a low LAI, still transpires (evaporate) significantly. Second, the results indicate that  $ET_a$  values may be comparable between grassed and forested areas, despite the much lower LAI values detected in the grasslands. This

assertion was supported by both spatial images in which slightly different or similar values of  $ET_a$  were detected between forested and grassed areas despite the large difference in LAI. Despite the overall good agreement between the TSEB model and the EC method, the application of the TSEB model requires more attention given the reduction in the a priori estimate of the  $\alpha$  Priestley-Taylor coefficient in forested areas (Komatsu, 2015). It is essential to note that the  $ET_a$  of the TSEB model is strongly influenced by a reduction in the  $\alpha$  coefficient in the forests; therefore, spatially distributed values of  $ET_a$  may not correlate with LST, as shown in Figs. 13 and 14, where LST was greater in grassed areas than in surrounding forested areas. For this reason, we propose a more detailed study regarding the accurate quantification of the  $\alpha$  coefficient according to Komatsu (2005) in forested areas.

The evaporative fraction and Bowen ratio are useful indicators because they can provide information about the relationship between water stress and evaporation and can be used to monitor the water stress of vegetation. The accurate detection of the evaporative fraction by spatially oriented models such as the TSEB or METRIC models can significantly improve water management and capture water stress in crops and forests. For this reason, a section that evaluates the evaporative fraction is an important part of this study, and it is also included in other studies that quantify water stress using remote sensing models (Anderson et al., 2011; French, Hunsaker and Thorp, 2015; Aboutalebi et al., 2019; Kustas et al., 2019) or evaluate both models in the area of interest (Chirouze et al., 2014). The results for the evaporative fraction, as detected by the models and the EC method, indicate that most of the solar energy was converted into LE in the forest. This finding can correspond to the high level of vegetation cover in the floodplain forest and suggest a relatively significant cooling effect. Both models also showed agreement with the EC in terms of seasonal trend detection, revealing an increase in the evaporative fraction during the first half of the growing season and a slight decrease in the second half. Similarly, in both models, the lowest Bowen ratio values were detected in summer, and the maximum was detected in April in the forest. This indicates that available energy was mostly utilized in H during spring and mostly utilized in LE during the summer period. These seasonal trends may correspond to meteorological-surface conditions in summer, which necessitate greater transpiration from vegetation.

On the other hand, vegetation and meteorological conditions may not be as favorable for latent heat flux in September or April, leading to lower evaporative fraction values than those during the summer peak.

The results of the evaporative fraction and Bowen ratio detected by the TSEB model and partially by the METRIC model also indicate seasonal trends at the Grassland, but these results could be affected by seasonal variability due to grass cutting that takes place every growing season. However, both models indicate an increasing evaporative fraction during the growing season, with a maximum in September and a minimum in May. The results showed that most of the available energy was mostly utilized in LE during the second part of the growing season, while the lowest amount was utilized at the start of the season. The results from the Grassland demonstrate the highest values of the evaporative fraction and lowest values of the Bowen ratio during summer. This result should be related to the maximum vegetation cover and water availability, which corresponds to our expectations during the occurrence of these conditions in the summer periods when vegetation should be in full cover and have access to water, which is not present in deep layers in floodplain-grassland ecosystems.

## **6 Conclusion**

This study focused on evaluating two satellite-oriented models for quantifying  $ET_a$  and energy fluxes in the hydrologically unique ecosystem of the floodplain area of Central Europe. The strong motivation behind this study is the precise determination of the water balance under the conditions of Central Europe in connection with adaptation and mitigation measures against the negative impacts of climate change. The comparison demonstrated good agreement between the diagnostic models and the EC method at both test sites, affirming the substantial potential of these methods for addressing various practical hypotheses and challenges associated with water balance. However, accurate detection of energy fluxes and  $ET_a$  remains a challenge for further study in forested areas, where precise quantification of physical parameters, such as the Priestley-Taylor coefficient, is crucial.

## **Acknowledgement**

The authors acknowledge support from AdAgriF - Advanced methods of greenhouse gases emission reduction and sequestration in agriculture and forest landscape for climate change mitigation (CZ.02.01.01/00/22\_008/0004635).

L. Homolová was supported by grant TO01000345 “Forest functions in the past, present and future - what can society expect from forests under climate change?” from Norway and Technology Agency of the Czech Republic within the KAPPA programme.

T. Ghisi was financially supported by the Internal Grant Agency of the Faculty of AgriSciences at Mendel University in Brno as part of the research project no. AF-IGA2022-IP-033 “The effect of vegetation cover on hydrological processes in the Svatka River catchment”.

Z. Žalud contribution to the study was supported by the PERUN TAČR project no. SS02030040.

## References:

- Aboutalebi, M., Torres-Rua, A. F., McKee, M., Kustas, W. P., Nieto, H., Alsina, M. M., ... & Dokoozlian, N. (2019). Incorporation of unmanned aerial vehicle (UAV) point cloud products into remote sensing evapotranspiration models. *Remote sensing*, 12(1), 50.
- Allen, R. G., Tasumi, M., & Trezza, R. (2007a). Satellite-based energy balance for mapping evapotranspiration with internalized calibration (METRIC)—Model. *Journal of irrigation and drainage engineering*, 133(4), 380 – 394.
- Allen, R. G., Tasumi, M., Morse, A., Trezza, R., Wright, J. L., Bastiaanssen, W., ... & Robison, C. W. (2007b). Satellite-based energy balance for mapping evapotranspiration with internalized calibration (METRIC)—Applications. *Journal of irrigation and drainage engineering*, 133(4), 395 – 406.
- Anderson, M. C., Norman, J. M., Diak, G. R., Kustas, W. P., & Mecikalski, J. R. (1997). A two-source time integrated model for estimating surface fluxes using thermal infrared remote sensing. *Remote sensing of environment*, 60(2), 195-216, [https://doi.org/10.1016/S0034-4257\(96\)00215-5](https://doi.org/10.1016/S0034-4257(96)00215-5)
- Anderson, M. C., Hain, C., Wardlow, B., Pimstein, A., Mecikalski, J. R., & Kustas, W. P. (2011). Evaluation of drought indices based on thermal remote sensing of evapotranspiration over the continental United States. *Journal of Climate*, 24(8), 2025 – 2044.
- Anderson, M. C., Allen, R. G., Morse, A., & Kustas, W. P. (2012). Use of Landsat thermal imagery in monitoring evapotranspiration and managing water resources. *Remote Sensing of Environment*, 122, 50 – 65.
- Brutsaert, W., & Sugita, M. (1992). Application of self-preservation in the diurnal evolution of the surface energy budget to determine daily evaporation. *Journal of Geophysical Research: Atmospheres*, 97(D17), 18377 – 18382.
- Burchard-Levine, V., Nieto, H., Kustas, W. P., Gao, F., Alfieri, J. G., Prueger, J. H., ... & Dokoozlian, N. (2022). Application of a remote-sensing three-source energy balance model to improve evapotranspiration partitioning in vineyards. *Irrigation Science*, 40(4-5), 593 – 608.

- Bastiaanssen, W. G., Pelgrum, H., Wang, J., Ma, Y., Moreno, J. F., Roerink, G. J., & Van der Wal, T. (1998). A remote sensing surface energy balance algorithm for land (SEBAL): Part 2: Validation. *Journal of hydrology*, 212, 213-229.
- Bastiaanssen, W. G. M., Noordman, E. J. M., Pelgrum, H., Davids, G., Thoreson, B. P., & Allen, R. G. (2005). SEBAL model with remotely sensed data to improve water-resources management under actual field conditions. *Journal of irrigation and drainage engineering*, 131(1), 85 – 93.
- Bhattarai, N., Quackenbush, L. J., Im, J., & Shaw, S. B. (2017). A new optimized algorithm for automating endmember pixel selection in the SEBAL and METRIC models. *Remote sensing of environment*, 196, 178-192.
- Carrasco-Benavides, M., Ortega-Farías, S., Lagos, L. O., Kleissl, J., Morales-Salinas, L., & Kilic, A. (2014). Parameterization of the satellite-based model (METRIC) for the estimation of instantaneous surface energy balance components over a drip-irrigated vineyard. *Remote Sensing*, 6(11), 11342 – 11371.
- Choi, M., Kustas, W. P., Anderson, M. C., Allen, R. G., Li, F., & Kjaersgaard, J. H. (2009). An intercomparison of three remote sensing-based surface energy balance algorithms over a corn and soybean production region (Iowa, US) during SMACEX. *Agricultural and Forest Meteorology*, 149(12), 2082 – 2097.
- Chirouze, J., Boulet, G., Jarlan, L., Fieuzal, R., Rodriguez, J. C., Ezzahar, J., ... & Chehbouni, G. (2014). Intercomparison of four remote-sensing-based energy balance methods to retrieve surface evapotranspiration and water stress of irrigated fields in semi-arid climate. *Hydrology and earth system sciences*, 18(3), 1165 – 1188.
- Choragudi, V. N. R. K. (2011). Sensitivity analysis on mapping evapotranspiration at high resolution using internal calibration (METRIC).
- Duethmann, D., & Blöschl, G. (2018). Why has catchment evaporation increased in the past 40 years? A data-based study in Austria. *Hydrology and Earth System Sciences*, 22(10), 5143 – 5158.

Dubayah, R.O., S.B. Luthcke, T.J. Sabaka, J.B. Nicholas, S. Preaux, and M.A. Hofton. 2021. GEDI L3 Gridded Land Surface Metrics, Version 2. ORNL DAAC, Oak Ridge, Tennessee, USA.

ESA. CORINE Land Cover 2018. Available at: <https://doi.org/10.2909/71c95a07-e296-44fc-b22b-415f42acfd0>. online (accessed on 10 July 2023).

Fischer, M., Zenone, T., Trnka, M., Orság, M., Montagnani, L., Ward, E. J., ... & Ceulemans, R. (2018). Water requirements of short rotation poplar coppice: Experimental and modelling analyses across Europe. *Agricultural and Forest Meteorology*, 250, 343 – 360.

Fischer, M., Pavlík, P., Vizina, A., Bernsteinová, J., Parajka, J., Anderson, M., ... & Trnka, M. (2023). Attributing the drivers of runoff decline in the Thaya river basin. *Journal of Hydrology: Regional Studies*, 48, 101436.

Foken, M. Göckede, M. Mauder, L. Mahrt, B.D. Amiro, W.J. Munger. Post-field data quality control. X. Lee, W.J. Massmann, B. Law (Eds.), *Handbook of Micrometeorology: A Guide for Surface Flux Measurements and Analysis*, Kluwer, Dordrecht (2004), pp. 181 – 208.

Foken, T. (2008). *Micrometeorology* (p. 308). Berlin/Heidelberg: Springer.

Foken, T., & Foken, T. (2017). Experimental methods for estimating the fluxes of energy and matter. *Micrometeorology*, 143 – 205.

French, A. N., Hunsaker, D. J., & Thorp, K. R. (2015). Remote sensing of evapotranspiration over cotton using the TSEB and METRIC energy balance models. *Remote Sensing of Environment*, 158, 281 – 294.

Ghisi, T., Fischer, M., Kowalska, N., Jocher, G., Orság, M., Bláhová, M., ... & Trnka, M. (2023). Faster evapotranspiration recovery compared to canopy development post clearcutting in a floodplain forest. *Forest Ecology and Management*, 532, 120828.

Guzinski, R., Anderson, M. C., Kustas, W. P., Nieto, H., & Sandholt, I. (2013). Using a thermal-based two source energy balance model with time-differencing to estimate surface energy fluxes with day–night MODIS observations. *Hydrology and Earth System Sciences*, 17(7), 2809 – 2825.

- Guzinski, R., & Nieto, H. (2019). Evaluating the feasibility of using Sentinel-2 and Sentinel-3 satellites for high-resolution evapotranspiration estimations. *Remote sensing of Environment*, 221, 157 – 172.
- Guzinski, R., Nieto, H., Sandholt, I., & Karamitilios, G. (2020). Modelling high-resolution actual evapotranspiration through Sentinel-2 and Sentinel-3 data fusion. *Remote Sensing*, 12(9), 1433.
- Guzinski, R., Nieto, H., Sánchez, R. R., Sánchez, J. M., Jomaa, I., Zitouna-Chebbi, R., ... & López-Urrea, R. (2023). Improving field-scale crop actual evapotranspiration monitoring with Sentinel-3, Sentinel-2, and Landsat data fusion. *International Journal of Applied Earth Observation and Geoinformation*, 125, 103587.
- Gurney, R. J., & Hsu, A. Y. (1990, January). Relating evaporative fraction to remotely sensed data at the FIFE site. In *Symposium on FIFE-First ISLSCP Field Experiment*.
- Hankerson, B., Kjaersgaard, J., & Hay, C. (2012). Estimation of evapotranspiration from fields with and without cover crops using remote sensing and in situ methods. *Remote Sensing*, 4(12), 3796 – 3812.
- Hlásny, T., Mátyás, C., Seidl, R., Kulla, L., Merganičová, K., Trombik, J., ... & Konôpka, B. (2014). Climate change increases the drought risk in Central European forests: What are the options for adaptation?. *Central European Forestry Journal*, 60(1), 5 – 18.
- Kalma, J. D., & Jupp, D. L. B. (1990). Estimating evaporation from pasture using infrared thermometry: evaluation of a one-layer resistance model. *Agricultural and Forest Meteorology*, 51(3-4), 223 – 246.
- Kustas, W. P., & Norman, J. M. (1999). Evaluation of soil and vegetation heat flux predictions using a simple two-source model with radiometric temperatures for partial canopy cover. *Agricultural and Forest Meteorology*, 94(1), 13 – 29.
- Kustas, W. P., Li, F., Jackson, T. J., Prueger, J. H., MacPherson, J. I., & Wolde, M. (2004). Effects of remote sensing pixel resolution on modeled energy flux variability of croplands in Iowa. *Remote sensing of Environment*, 92(4), 535 – 547.
- Kustas, W. P., Nieto, H., Morillas, L., Anderson, M. C., Alfieri, J. G., Hipps, L. E., ... & Garcia, M. (2016). Revisiting the paper “Using radiometric surface temperature for surface energy flux estimation

in Mediterranean drylands from a two-source perspective”. *Remote Sensing of Environment*, 184, 645 – 653.

Kustas, W. P., Alfieri, J. G., Nieto, H., Wilson, T. G., Gao, F., & Anderson, M. C. (2019). Utility of the two-source energy balance (TSEB) model in vine and interrow flux partitioning over the growing season. *Irrigation Science*, 37, 375 – 388.

Komatsu, H. (2005). Forest categorization according to dry-canopy evaporation rates in the growing season: comparison of the Priestley–Taylor coefficient values from various observation sites. *Hydrological Processes: An International Journal*, 19(19), 3873 – 3896.

Komissarov, M. A., & Klik, A. (2020). The impact of no-till, conservation, and conventional tillage systems on erosion and soil properties in Lower Austria. *Eurasian soil science*, 53, 503 – 511.

Liebert, R., Huntington, J., Morton, C., Sueki, S., & Acharya, K. (2016). Reduced evapotranspiration from leaf beetle induced tamarisk defoliation in the Lower Virgin River using satellite-based energy balance. *Ecohydrology*, 9(1), 179 – 93.

Long, D., & Singh, V. P. (2013). Assessing the impact of end-member selection on the accuracy of satellite-based spatial variability models for actual evapotranspiration estimation. *Water Resources Research*, 49(5), 2601 – 2618.

Mkhwanazi, M., Chávez, J. L., & Andales, A. A. (2015). SEBAL-A: A remote sensing ET algorithm that accounts for advection with limited data. Part I: Development and validation. *Remote Sensing*, 7(11), 15046 – 15067.

Mozny, M., Trnka, M., Vlach, V., Vizina, A., Potopova, V., Zahradnicek, P., ... & Zalud, Z. (2020). Past (1971–2018) and future (2021–2100) pan evaporation rates in the Czech Republic. *Journal of Hydrology*, 590, 125390.

Morton, C. G., Huntington, J. L., Pohl, G. M., Allen, R. G., McGwire, K. C., & Bassett, S. D. (2013). Assessing calibration uncertainty and automation for estimating evapotranspiration from agricultural areas using METRIC. *JAWRA Journal of the American Water Resources Association*, 49(3), 549 – 562.

- Nieto, H., Kustas, W. P., Torres-Rúa, A., Alfieri, J. G., Gao, F., Anderson, M. C., ... & McKee, L. G. (2019a). Evaluation of TSEB turbulent fluxes using different methods for the retrieval of soil and canopy component temperatures from UAV thermal and multispectral imagery. *Irrigation Science*, 37, 389 – 406.
- Nieto, H., Kustas, W. P., Alfieri, J. G., Gao, F., Hipps, L. E., Los, S., ... & Anderson, M. C. (2019b). Impact of different within-canopy wind attenuation formulations on modelling sensible heat flux using TSEB. *Irrigation Science*, 37, 315 – 331.
- Norman, J. M., Kustas, W. P., & Humes, K. S. (1995). Source approach for estimating soil and vegetation energy fluxes in observations of directional radiometric surface temperature. *Agricultural and Forest Meteorology*, 77(3-4), 263 – 293.
- Olmedo, G. F., Ortega Farias, S., Fonseca Luengo, D., & Fuentes Peñailillo, F. (2016). Water: tools and functions to estimate actual evapotranspiration using Land Surface Energy Balance Models in R.
- Papale, D., Reichstein, M., Aubinet, M., Canfora, E., Bernhofer, C., Kutsch, W., ... & Yakir, D. (2006). Towards a standardized processing of Net Ecosystem Exchange measured with eddy covariance technique: algorithms and uncertainty estimation. *Biogeosciences*, 3(4), 571 – 583.
- Pastorello, G., Agarwal, D., Papale, D., Samak, T., Trotta, C., Ribeca, A., ... & Canfora, E. (2014, October). Observational data patterns for time series data quality assessment. In *2014 IEEE 10th International Conference on e-Science* (Vol. 1, pp. 271 – 278). IEEE.
- Peddinti, S. R., & Kisekka, I. (2022). Estimation of turbulent fluxes over almond orchards using high-resolution aerial imagery with one and two-source energy balance models. *Agricultural Water Management*, 269, 107671.
- Potapov, P., Li, X., Hernandez-Serna, A., Tyukavina, A., Hansen, M. C., Kommareddy, A., ... & Hofton, M. (2021). Mapping global forest canopy height through integration of GEDI and Landsat data. *Remote Sensing of Environment*, 253, 112165.

- Pozníková, G., Fischer, M., van Keulen, B., Orság, M., Hlavinka, P., Žalud, Z., & Trnka, M. (2018). Quantifying turbulent energy fluxes and evapotranspiration in agricultural field conditions: A comparison of micrometeorological methods. *Agricultural water management*, 209, 249 – 263.
- Reichstein M et al. 2005 On the separation of net ecosystem exchange into assimilation and ecosystem respiration: review and improved algorithm. *Glob. Change Biol.* 11, 1424-1439. (doi:10.1111/j.1365-2486.2005.001002.x) Crossref, ISI, Google Scholar
- Senay, G. B., Budde, M., Verdin, J. P., & Melesse, A. M. (2007). A coupled remote sensing and simplified surface energy balance approach to estimate actual evapotranspiration from irrigated fields. *Sensors*, 7(6), 979 – 1000.
- Sugita, M., & Brutsaert, W. (1991). Daily evaporation over a region from lower boundary layer profiles measured with radiosondes. *Water Resources Research*, 27(5), 747 – 752.
- Tasumi, M. (2003). *Progress in operational estimation of regional evapotranspiration using satellite imagery*. University of Idaho.
- Timmermans, W. J., Kustas, W. P., Anderson, M. C., & French, A. N. (2007). An intercomparison of the surface energy balance algorithm for land (SEBAL) and the two-source energy balance (TSEB) modeling schemes. *Remote Sensing of Environment*, 108(4), 369 – 384.
- Trnka, M., Bartošová, L., Grammatikopoulou, I., Havlík, P., Olesen, J. E., Hlavinka, P., ... & Žalud, Z. (2022a). The Possibility of Consensus Regarding Climate Change Adaptation Policies in Agriculture and Forestry among Stakeholder Groups in the Czech Republic. *Environmental Management*, 69(1), 128 – 139.
- Trnka, M., Vizina, A., Hanel, M., Balek, J., Fischer, M., Hlavinka, P., ... & Brázdil, R. (2022b). Increasing available water capacity as a factor for increasing drought resilience or potential conflict over water resources under present and future climate conditions. *Agricultural Water Management*, 264, 107460.

Twine, T. E., Kustas, W. P., Norman, J. M., Cook, D. R., Houser, P., Meyers, T. P., ... & Wesely, M. L. (2000). Correcting eddy-covariance flux underestimates over a grassland. *Agricultural and forest meteorology*, *103*(3), 279 – 300.

Weiss, M., Baret, F., Myneni, R., Pragnère, A., & Knyazikhin, Y. (2000). Investigation of a model inversion technique to estimate canopy biophysical variables from spectral and directional reflectance data. *Agronomie*, *20*(1), 3 – 22.

Zhang, C., Long, D., Zhang, Y., Anderson, M. C., Kustas, W. P., & Yang, Y. (2021). A decadal (2008–2017) daily evapotranspiration data set of 1 km spatial resolution and spatial completeness across the North China Plain using TSEB and data fusion. *Remote Sensing of Environment*, *262*, 112519.